Design of 3-DOF Parallel Manipulators for Micro-Motion Applications

By

JIAN LI

A Thesis Submitted in Partial Fulfillment

Of the Requirements for the Degree of

Master of Applied Science

in

The Faculty of Engineering and Applied Science

Mechanical Engineering Program

University of Ontario Institute of Technology

August, 2009

CERTIFICATE OF APPROVAL

Submitted by: **Jian** **Li** Student #: **100332892**
First Name, Last Name

In partial fulfillment of the requirements for the degree of:

Master of Applied Science in Mechanical Engineering

Degree Name in full (e.g. Master of Applied Science) Name of Program

Date of Defense (if applicable): _____

Thesis Title:

Design of 3-DOF Parallel Manipulators for Micro-Motion Applications

The undersigned certify that they recommend this thesis to the Office of Graduate Studies for acceptance:

Chair of Examining Committee	Signature	Date (yyyy/mm/dd)
External Examiner	Signature	Date (yyyy/mm/dd)
Member of Examining Committee	Signature	Date (yyyy/mm/dd)
Member of Examining Committee	Signature	Date (yyyy/mm/dd)

As research supervisor for the above student, I certify that I have read the following defended thesis, have approved changes required by the final examiners, and recommend it to the Office of Graduate Studies for acceptance:

Name of Research Supervisor	Signature of Research Supervisor	Date (yyyy/mm/

Abstract

This thesis presents two unique micro-motion parallel kinematic manipulators (PKM): a three degrees of freedom (3-DOF) micro-motion manipulator and a 3-DOF micro-motion manipulator with actuation redundancy. The 3-DOF micro-motion manipulator has three linear-motion driving units, and the 3-DOF micro-motion manipulator with redundancy has four of these units.

For both designs, the linear motion driving units are identical, and both machines have a passive link in the center of the structure. The purpose of this passive link is to restrain the movement of the manipulator and to improve the stiffness of the structure. As a result, both structures support 3-DOF, including one translation on the Z-axis and two rotations around the X and Y axes. The manipulator with redundancy is designed to prevent singularity and to improve stiffness.

In this thesis, the inverse kinematic, Jacobian matrix and stiffness analyses have been conducted, followed by the design optimization for structures. Finally, the FEA (Finite Element Analysis) and dynamic analysis have also been performed.

There are many practical applications for micro-motion parallel manipulators. The typical applications include micro-machine assembly, biological cell operation, and micro-surgery .

Acknowledgements

First, I would like to acknowledge Dr. Dan Zhang for giving me the opportunity to study and work under his supervision. He has been an excellent advisor, as I have obtained the required scientific and engineering knowledge, and I have discovered new ways to perceive situations and to solve problems with his guidance. Dr. Zhang has been an invaluable resource; he is my teacher, my mentor, and also my friend.

Also, I wish to thank all the fellows with whom I have studied. In particular, I would like to give my special thanks to Qi Shi, who provided wonderful support, and whom without, I could not be successful in completing this thesis. I also want to thank my family, especially my wife, my parents, my sister and my friends, who supported and encouraged me throughout my studies.

Contents

List of Figures

List of Tables

List of Acronyms

DOF:	Degrees of Freedom
FEA:	Finite Element Analysis
GA:	Genetic Algorithms
PKM:	Parallel Kinematic Manipulator
PZT:	Piezoelectric Action
SKM:	Serial Kinematic Manipulator
PRS:	Prismatic, Revolute and Spherical Joint

Chapter 1

Introduction

1.1 Literature review

There is an abundance of research on the Parallel Kinematic Manipulator (PKM), most of which examines either the Micro Machine or Micro Motion Structures [1, 2].

Recently, there has been an increasing trend in the research of micro machines, as industries want to make current machines smaller, more energy-efficient and precise. For instance, Liu [3] has developed an intelligent micromanipulator based on 3-PRS in parallel mechanisms. Moreover, Harashima [4] has introduced a new type of integrated micro-motion systems Bang [5] designed a micro parts assembly system with a micro gripper, and Zubir [6] expanded on this research to present a newly developed high-precision micro gripper. Finally, Gilsinn [7] focused on a macro-micro motion system for a scanning, tunneling microscope.

There are many benefits of micro machines, especially in comparison to regular machines. For instance, they are relatively small, they have a higher precision and they consume much less energy than a regular machine. These characteristics make micro machines popular in the fields of information and telecommunications, medicine, biotechnology, and the automotive industry. Specifically, micro machines are regarded as a vital component for strengthening international competition in major areas of the manufacturing industry [8]. Applications related to these machines are expected to be in high demand by many companies in the near future. [9].

The application of the micro machine tool, especially with its high degrees of precision and speed, provides significant benefits for the manufacturer. Specifically, it can help to increase the accuracy and precision in production, and the recent trends towards high-speed micro machining have been a very popular field of research in developing new types of parallel kinematics machines [10].

Three Degrees of Freedom (DOF) is the basic requirement for the parallel kinematics machines. Since most machine operations only require a maximum of 5 axes, new configurations with less than six parallel axes would be appropriate for these operations [11]. A substantial amount of research has been conducted on the 3-DOF parallel kinematics manipulator. For example, Clavel [12] and Sternheim [13] reported a 3-DOF high-speed

robot known as the Delta Robot, while Lee and Shah [14] analyzed a 3-DOF parallel manipulator. Some 3-DOF parallel manipulator architectures provide a pure relative rotation of the moving platform and are used as point devices, manipulator wrists and orienting devices [15, 16]. Tsai [17, 18] introduced a novel 3-DOF translation moving platform, which is comprised of only revolute joints and performs pure translational motion. To improve the stiffness of the 3-DOF PKM, Zhang [19, 20] proposed a passive link structure, which increases the stiffness of the system. These research discoveries provide the foundations for the 3-DOF PKM.

The 3-DOF Micro-Motion Parallel Manipulator can be applied to precision manufacturing and assembly for small parts ranging in size from millimeters to micrometers. Micro Machine Tools are in demand worldwide, and their popularity will also turn Micro Motion Mechanisms into machines that can perform small motions and have very high accuracy. In the subsequent sections, serial and parallel kinematic manipulators will be introduced, then micro motion structures will be discussed, and finally, the new design of micro motion structures will be described.

1.1.1 Serial Robotic Machine Tool

A serial robot is a serial mechanism with an open kinematic chain that is connected at its base and its end effectors [21]. The first robotics patents were applied for by an American inventor, George Charles Devol Jr., in 1954, and subsequently, they were granted in 1961. However, robotics was not widely used in the industry until the early 1970's, when robots were utilized to replace human workers in monotonous and hazardous work environments by companies such as General Electric and General Motors. Today, serial mechanisms are extensively used in a wide variety of industrial areas. Some typical robotic applications include welding, painting, assembly, pick and place, packaging, product inspecting, and testing. There are many advantages to using robots, including a very large working area in comparison to the size of the mechanism itself, and the relative ease of analyzing their structure and range of motion.

Most conventional machine tools are designed based on the serial structure. However, the existence of an open kinematic chain creates a number of disadvantages. First, it is difficult to achieve a high degree of accuracy, since the system accumulates the individual errors of sequentially linked components. Secondly, the cost of energy is expensive, since heavy actuators, which drive the moving components directly or through a transmission

device, need to be installed on each component. Finally, their machining speed is limited, since the system stiffness or rigidity is relatively low, causing the occurrence of vibration and instability, thus resulting in lower efficiency and accuracy. Therefore, open kinematic chains diminish the acceleration and speed, decrease the dynamic performance, and limit the system stiffness at the end effector. As well, the load, forces, and weight of the upper axis must be supported by the lower axis, which results in the poor dynamic behaviors of the lower axis [22]. Overall, the limited performance of serial mechanisms demonstrates that they are unsuitable for use as a precision micro motion manipulator.

The following illustrations compare the typical applications of a serial robot and a conventional machine tool.

igure 1.1: Serial Robot and Conventional Machine Tool

1.1.2 Parallel Robotic Machine Tool

A parallel kinematic manipulator (PKM) is a closed-loop mechanism, where a moving platform is connected to the base by at least two serial kinematic chains, or legs [21]. The PKM has enormous potential for overcoming the disadvantages of serial robots. First, this device is more accurate, since its moving components are more strongly related and the link errors are not accumulated. Furthermore, it is much more rigid than a serial robot, as the same end-effectors are simultaneously supported by at least two kinematic chains. Lastly, it has a much lighter moving mass, as all of the actuators are mounted on the base, allowing it to function at a higher speed and with greater precision.

The first conventional Stewart Platform (SP) kinematic manipulator was designed by Gough [19]; it has six extensible legs and hence a very rigid kinematic structure. This system consists of six linear actuators independently driven by six stepper motors. It can perform translational movements and be implemented in precision engineering applications. In comparison to the serial kinematic manipulator (SKM), the parallel kinematic manipulator has the desirable characteristics of greater payload and rigidity, more precision, and higher speed and acceleration. On the other hand, the disadvantages of the PKM include a limited working envelope as well as more complex direct kinematics and control algorithms.

The parallel robot has the following advantages in comparison with the serial manipulator:

- High accuracy due to non-cumulative joint errors
- High force/ torque capacity since the load is evenly distributed
- Structural rigidity and stiffness

Therefore, parallel robots are suitable for applications in which high speed, high positioning accuracy, and a rapid dynamic response are required.

Figure 1.2: Exechon X700 Transparent (Courtesy of Exechon AB of Sweden)

This design, which consists of two active moving pods and one passive pod, is patented by Exchon AB of Sweden, and it has been used for CNC machine tool heads.

1.2 Parallel Robot Based Micro Motion Systems

1.2.1 Introduction and Applications

Precise micro-motion manipulation has become increasingly important in many applications, such as small parts precision machining, chip assembly in the semiconductor industry, cell manipulation in biotechnology, and automatic surgery. The micro-motion system has been strongly recommended by researchers around the world, as it its materials are less expensive and it is more energy efficient, and thus, this system represents the current development direction in engineering.

At the same time, the advanced fabrication technique enables the miniaturization of existing parallel robotic systems, whose motion ranges can vary from a few millimeters to micrometers. The advantages of the micro-motion parallel kinematic manipulator can be summarized in the following points [23, 24]:

- Lower Inertia
- Improved Dynamic Behavior
- High Speed and Acceleration
- Smaller Package Size
- Greater Stiffness

- Increased Repeatability and Reliability

The following illustration shows an example of the parallel kinematics manipulator used in precision machining. This device is conventionally designed for specific functions, such as the fabrication of watch parts and engraving.

Figure 1.3: Desktop Micro CNC Machine KOSY3 A5 (Courtesy of MAX computer GmbH, Germany)

1.2.2 Existing Micro Motion Systems

As discussed in Section 1.2.1, there are many micro-motion structures that have been designed and analyzed by researchers. Based on their defining characteristics, these machines can be divided into two main types. The first type of micro-motion structure is a miniaturized device that is driven by tiny actuators. Overall, the mechanism is usually less than one cubic foot, and its motion range can vary from several micrometers to several centimeters.

The second type of micro motion system is a nano-positional micro motion manipulator, also known as the piezoelectric (PZT). Generally, the actuation element of this motion system is integrated with the compliant micro-motion system, and it can achieve high degrees of stiffness and accuracy. However, according to their actuators, the motion ranges of this system are within 0 to 1000 μm [8]. Figure 1.4 demonstrates a conventional micro PKM, which is successfully used in medical surgery.

Figure 1.4: Hexapod Robots in Spinal Surgery (Courtesy of Mazor Surgical Technologies)

This hexapod robot is 50mm, or 2 inches, in diameter and 80mm, or 3.15 inches, in height, with a weight of 250g, or 0.5 lb. According to a pre-operational plan, it is able to automatically position itself at an exact location, and it serves as a guiding tool for surgery, especially when the surgeon drills or performs an operation on a bone. This invention has been approved by the FDA (US Food and Drug Administration) and the CE (European Conformity).

Another example of a micro-motion system is the Compliant Mechanism. “A compliant mechanism is a mechanism that is composed of at least one component that is sensibly deformable compared to the other rigid links. The compliant mechanisms, therefore, gain their mobility by transforming an input form of energy into output motion” [22]. Hence,

they are flexible mechanisms that transfer an input force or a displacement to another point through the elastic body deformation of their flexible joints. Piezoelectric actuators (PZT) are used in compliant machine structures for linear motion. They can develop a linear motion on driving element and flexure pivots, which can receive a resolution range of 10 pm ($1pm = 10^{-12}m$) to 100 um [8]. There are many companies that are making the micro-motion systems, such as ALIO Industries and PI (Physik Instrumente).

Figure: 1.5 ALIO HR2 Hexapod (Courtesy of ALIO Industries)

As shown above, the ALIO hexapod with a six nanometer resolution revolves around a virtual point in space and has a maximum speed of 250 mm/s.

Some applications have special requirements, such as limited space for installation and workspace requirements that are much larger than applications with a nano-scale structure. For instance, nano-lithography does not have the capability of developing a large work area. The newly developed designs intend to meet these two objectives, as this micro-motion manipulator has been used successfully in areas such as jewelry engraving and micro-precision machining for electronic circuits.

The illustrations below, Figures 1.6 and 1.7, show the first three-DOF micro-motion parallel manipulator proposed in this thesis.

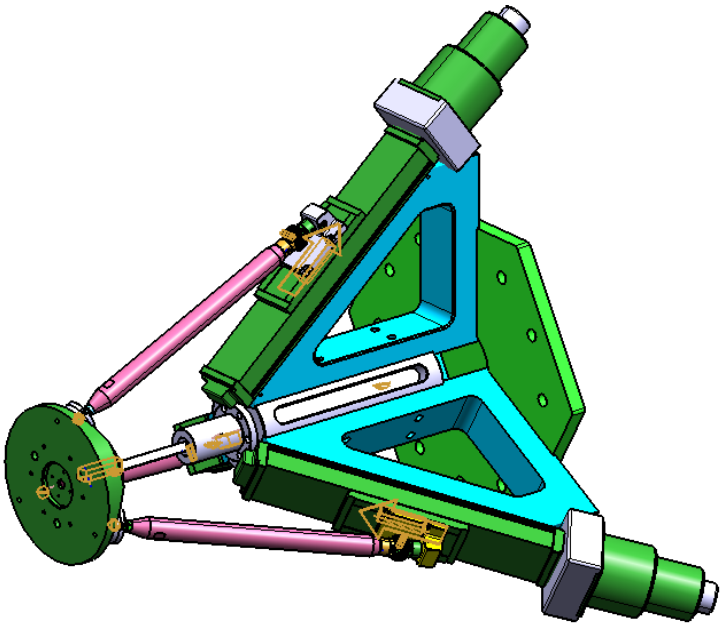

Figure 1.6: New CAD Model

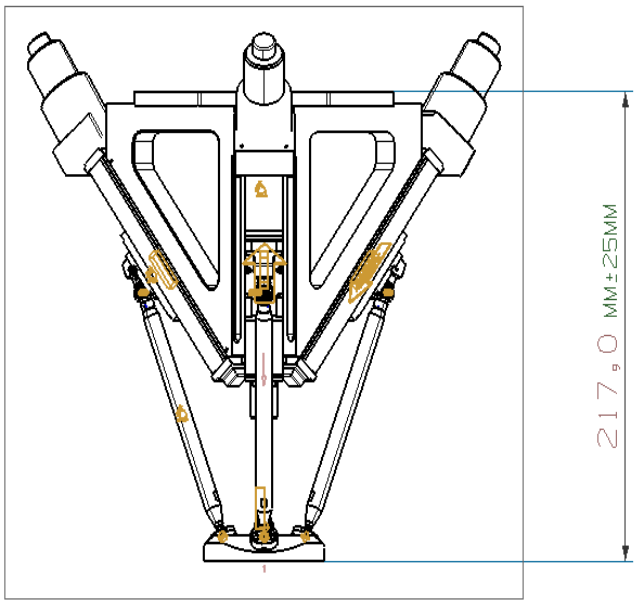

Figure 1.7: The Dimensions of the Newly Designed Micro-Motion Parallel Manipulator

MM ±25 MM assembly height at middle of z stroke range (z stroke = 50mm)

This research examines the feasibility of two novel 3-DOF parallel manipulators used for machining applications. The unique design of these manipulators aims at achieving higher stiffness and greater 3-DOF motion by eliminating all side-effect motions. These manipulators consist of three or four identical legs with active actuators, or driving motors, which accomplish their movement through the motion of precision ball screws. Each of the actuated legs is connected to the moving platform by a spherical joint, and both manipulators have one passive leg installed between the base and the moving platform. The passive link

can only have linear motion on the middle platform, while the other end is connected to the moving platform by a universal joint, eliminating the rotation of the z-axis.

1.2.3 The Organization of the Thesis

Chapter 2 presents the concept design for the novel 3-DOF Micro-Motion Parallel Manipulators. Specifically, several concepts detailing kinematic structure development are addressed. Subsequently, Chapter 3 focuses on the kinematic analysis of the 3-DOF Micro-Motion Parallel Manipulator with a passive leg, and Chapter 4 discusses the kinematic analysis of the 3-DOF Actuation Redundant Micro-Motion Parallel Manipulator. Next, Chapter 5 describes the optimization result of these two 3-DOF Micro-Motion Parallel Manipulators. Chapter 6 presents the simulations, comparisons and the results of Finite Element Analysis, as well as the result of Velocity and Acceleration Analysis. Finally, Chapter 7 highlights the most important conclusions and observations of the study and suggests ideas for future work.

Chapter 2

The Novel Three Degrees of Freedom Micro Motion System

2.1 Description of the New Micro-Motion 3-DOF Parallel Manipulators

Two types of micro-motion 3-DOF parallel kinematic manipulators are proposed in this thesis: one kind contains three active links, and the other has four active links, which is known as a redundant parallel manipulator. Both manipulators have a passive link that is connected by a moving platform and a fixed base. Their active links are manipulated by a high-precision ball screw that controls linear motion units and provides high speed as well as a rapid response for the moving platform. Accordingly, Figures 2.1 and 2.2 represent two 3-DOF novel parallel manipulator CAD models.

The first 3-DOF parallel kinematic manipulator, known as 3-DOF PKM, is shown in Figure 2.1. This manipulator consists of four kinematic chains, including three actuated

moving links with an identical topology, and one passive constraining link connecting the fixed base to a moving platform. The three actuated moving links are designed as PUS (Prismatic - Universal – Spherical) Joints. The passive constraining link, which connects the base center to the platform center, consists of a prismatic joint and a universal joint attached to the moving platform. This last leg is used to constrain the motion around the z-axis rotation of the platform to only three degrees of freedom.

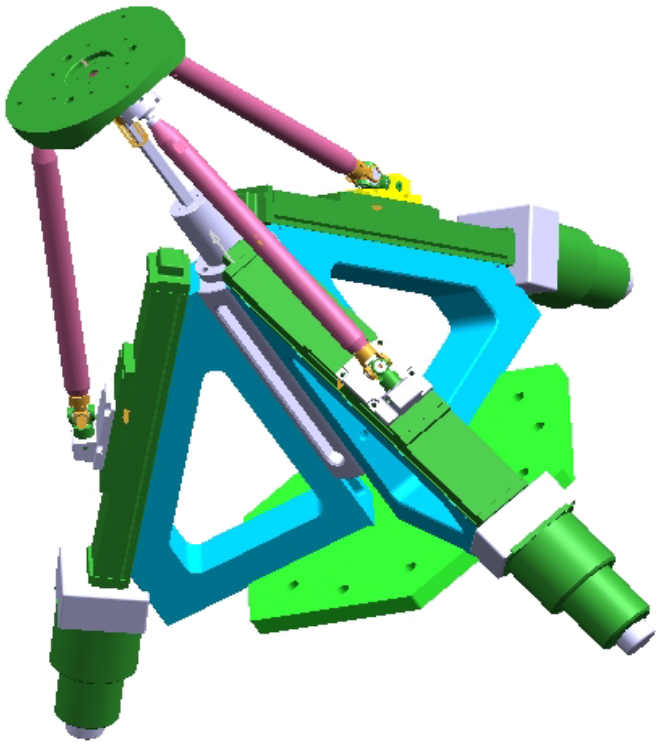

Figure 2.1: 3-DOF Micro Motion Manipulator Model

The second type of unique manipulator is an actuation redundant 3-DOF parallel manipulator, as shown in Figure 2.2. It consists of five kinematic chains, including four actuated moving links with an identical topology, and one passive constraining link connecting the fixed base to a moving platform. The moving platform has two rotations, which are along the x-axis and the y-axis, and one translation, which is along the z-axis.

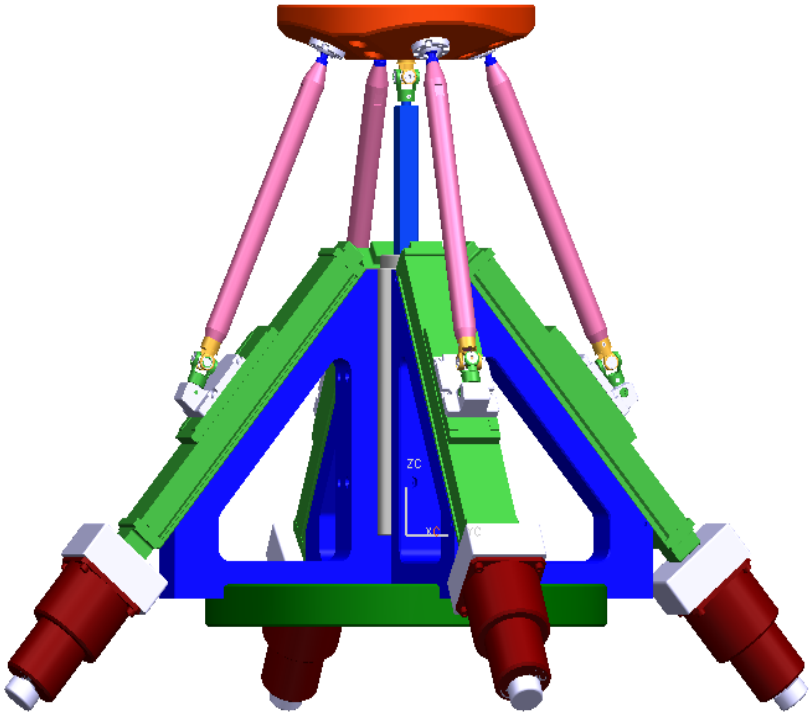

Figure 2.2: 3-DOF Micro Motion Manipulator with Actuation Redundancy

These two proposed models can be utilized for many practical applications, since their design is very flexible. For example, the size and the shape of the moving plate and the

base may have to be changed depending on the actual use, and the active driving motors or actors can also be modified for the installation. The following figures depict two examples of potential modifications.

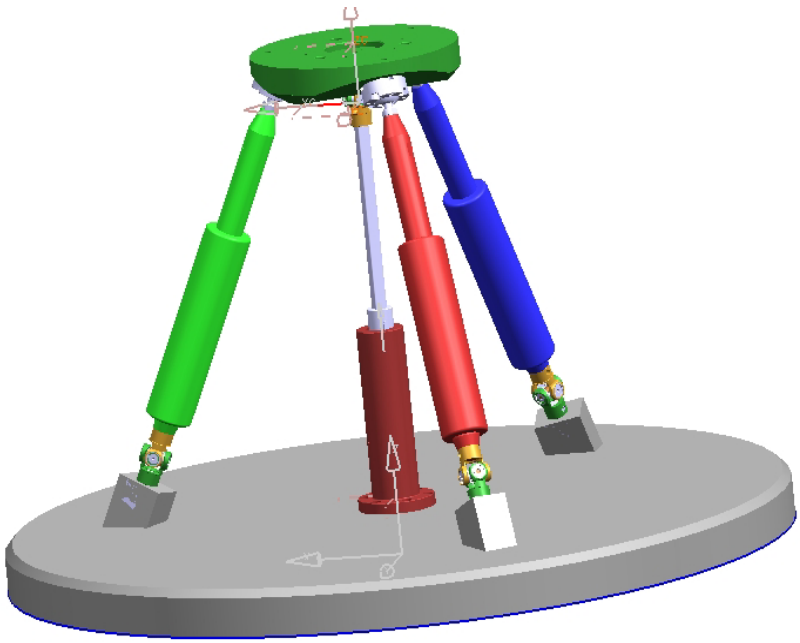

Figure 2.3: Derivation of CAD Model (Three legs)

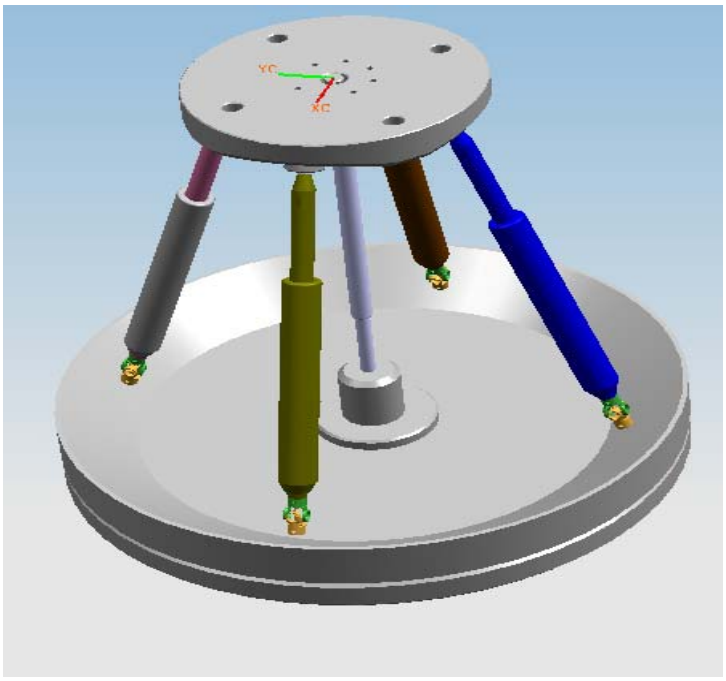

Figure 2.4: Derivation of CAD Model (Four Legs) Redundant Structure

2.2 Advantages of the New Micro-Motion Parallel Manipulator

- High degree of stiffness
- Functions in extremely difficult work environments, including high temperature, high humidity and intense vibration, where compliant structures cannot be used
- High speed and fast response
- Easily controlled
- Requires minimal maintenance

2.3 CAD Modeling Descriptions

As previously discussed, this thesis presents two types of models: the 3-DOF Micro-Motion Parallel Manipulator, which has three identical action links, or legs, and the 3-DOF redundant Micro-Motion Parallel Manipulator, which has four identical action links, or legs. Also, both models contain one constraining link, or passive leg. The diagram below demonstrates the first model, the 3-DOF Micro-Motion Parallel Manipulator. The components that have the same name in the 3-DOF Micro-Motion Redundant model have the same function as those in the 3-DOF Micro-Motion Parallel Manipulator.

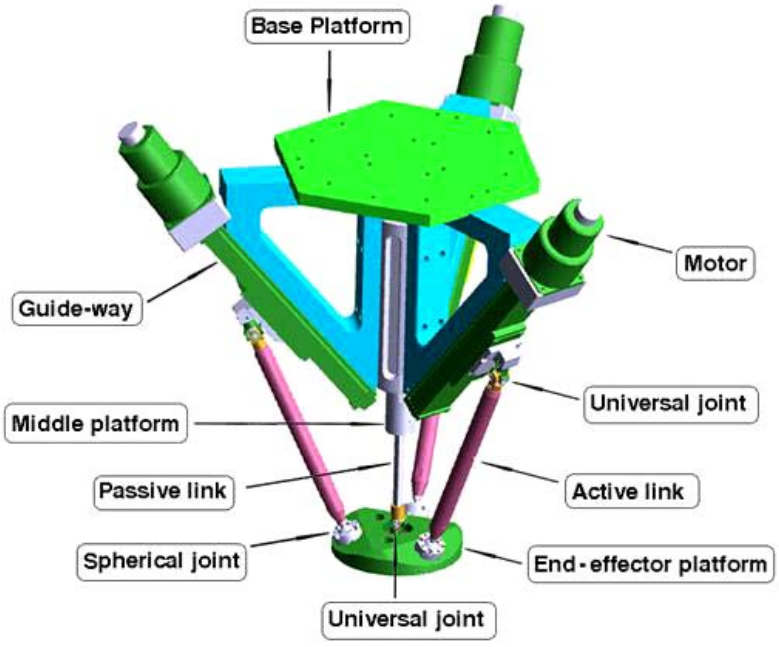

Figure 2.5: CAD Model with Components Description

In Figure 2.5, the micro-motion manipulator contains a base platform, an end-effector, or moving, platform, and three identical actuated links that are controlled by the motor through ball screws and the driving block. The actuated link is connected at one end with a driving block, which slides on a guide-way. At one end of the link is a universal joint, and at the other end of the link is a spherical joint, which is connected to the end-effector platform. Additionally, three triangular blocks are arranged in 120-degree intervals around the axis of the base platform. Depending on the application, the end-effector may be attached to the end-effector platform, which is located at the bottom of the link mechanism.

2.4 Potential Applications

The newly-developed micro-motion manipulators have accomplished increasingly demanding tasks in fields where high speed and high precision are required. They can be modified for utilization as machine tool heads, and the tool heads can be attached to existing systems, such as CNC machines, robots and CMM, to expand their motion range and their dexterity [11, 26].

Hence, based on the design of these structures, this 3-DOF micro-motion manipulator has been constructed with a 50 mm stroke along the z-axis and a $\pm 50°$ rotation on the x-axis and

the y-axis. They also have a 125mm moving platform diameter and a 250mm base platform diameter; however, these specifications can be modified according to the individual requirements.

Some potential applications include:

- Watch industry
- Assembly of micro-motors
- Assembly of micro-sensors
- Assembly of micro-technological devices
- Packaged system
- Micro-optical benches
- Biological cell manipulation

The following figure shows the manipulator being utilized as a CNC Machine in high precision machining,

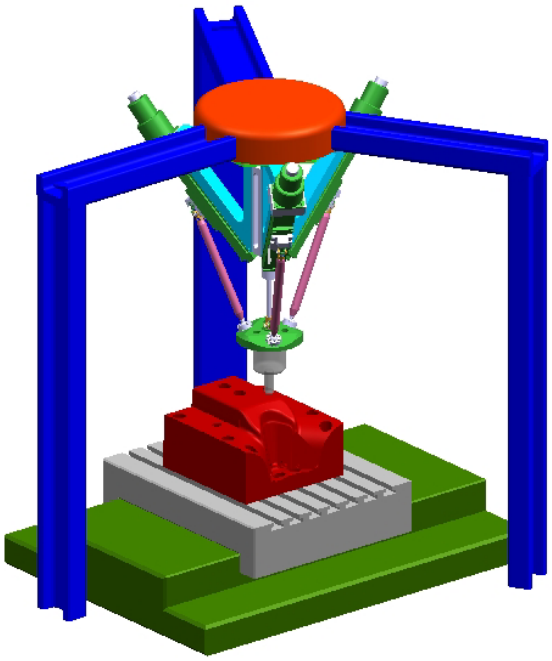

Figure 2.6: The Application as a CNC Machine

Chapter 3

Kinematic Modeling of the 3-DOF Micro Motion Manipulator

3.1 Kinematics Modeling

Unlike most existing 3-DOF parallel kinematic manipulator designs, the new design has improved the system's stiffness by using a passive leg which was connected the moving plate with a universal joint in the center of the moving platform [19, 20]. This design also eliminated the coupled motions at the reference point to simplify the kinematic model and the control.

As shown in Figure 3.1, this parallel manipulator includes a universal joint in the passive link. It is located on the moving platform rather than the base platform so that the motions along X and Y translations and Z rotation are eliminated.

The reference point is on the middle of the moving platform, which has uncoupled motion with X and Y rotations and Z translation. The proposed manipulator has three

platforms: base platform$B_1B_2B_3$, middle platform$m_1m_2m_3$, and moving platform $P_1P_2P_3$. The base platform is fixed on the ground. The middle platform is used to support guide-way B_im_i of actuated links D_iP_i .The moving platform is used to mount a tool. Actuated links D_iP_i are connected to the moving platform by a spherical joint (ball joint) at P_i, and to a slider connected to the active ball screw by a universal joint at D_i. The passive link is installed between the middle platform and the moving platform. The passive link with a prismatic joint is fixed on the middle platform at one end, and connected to the end-effector platform by a universal joint at the other end.

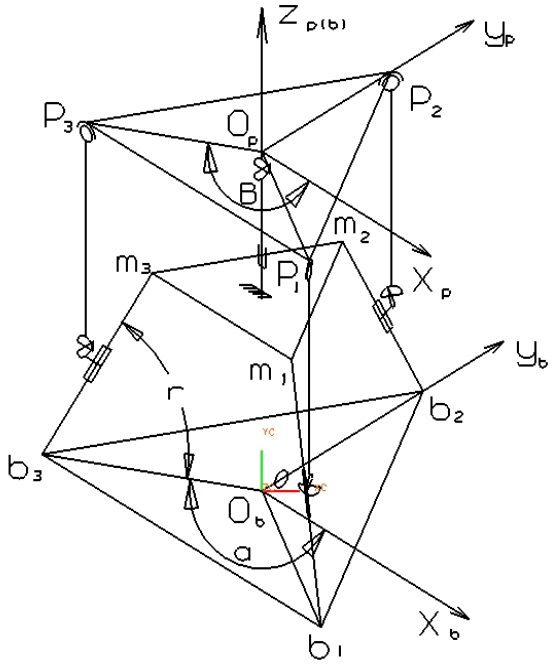

Figure 3.1 Schematic Model of 3 –DOF Micro Motion Parallel Manipulator Model

The following parameters define the details of the structure:

- the angle α_i (i=1,2,3) between X_b and O_bB_i ,
- the angle β_i (i = 1,2,3) between X_p and O_pP_i ,
- the distance from $O_b\ to\ B_i$ on the base platform is r_b,
- the distance from $O_p\ to\ P_i$ at the end-effector platform is r_p ,
- the angle of a guide-way γ,
- the length of an active link l_i , and
- the offset of the spherical joints on the platform Z_o.

To describe the structure of the 3-DOF manipulator, two coordinate systems, $\{O_p - X_pY_pZ_p\}$ and $\{O_b - X_bY_bZ_b\}$, are established, which are attached to the end- effector and base platform, respectively. For the origin O_p of the end-effector, its translational motions along X_p and Y_p, and rotational motion alongZ_p, are eliminated because of the usage of the passive leg, i.e.,

$$\begin{cases} x_p = y_p = 0 \\ \theta_z = 0 \end{cases} \tag{3-1}$$

Therefore, the motions of O_p can be denoted by $(\theta_x, \theta_y, \theta_z)$, where θ_x and θ_y are the rotational motions along X_p and Y_p, and Z_p is the translational motion alongZ_b. The position

of the end-effector with respect to the coordinate system $\{O_b - X_bY_bZ_b\}$ can be represented as following:

$$\boldsymbol{T_p^b} = \begin{bmatrix} \boldsymbol{R_p} & \boldsymbol{P_p} \\ \boldsymbol{0} & \boldsymbol{1} \end{bmatrix} = \begin{bmatrix} c\theta_y & 0 & s\theta_y & 0 \\ s\theta_x s\theta_y & c\theta_x & -s\theta_x c\theta_y & 0 \\ -c\theta_x s\theta_y & s\theta_x & c\theta_x c\theta_y & z_p \\ 0 & 0 & 0 & 1 \end{bmatrix} \quad (3\text{-}2)$$

Where

$\boldsymbol{C, S}$ are denoted the cosine and sine functions, respectively,

$\boldsymbol{T_p^b}$ is the pose of the end-effector with respect to the coordinate system$\{\boldsymbol{O_b - X_bY_bZ_b}\}$

$\boldsymbol{R_P}$ is the 3×3 orientation matrix of the end-effector,

$\boldsymbol{P_P}$ is the location of O_p.

3.2 Inverse Kinematics

The inverse kinematics is formulated by finding the joint motions when the pose of the end-effectors T_p^b is known. The joint motions are denoted by u_i and the pose of the end-effector T_p^b is determined by the motions of $O_p - (\theta_x, \theta_y, Z_P)$. To solve the inverse kinematic problem, one can apply the condition that the length of a support bar is constant.

The location of the connection between the end-effector platform and an active link is:

$$\boldsymbol{p}_{p_i}^{b} = \boldsymbol{R}_p \boldsymbol{p}_{p_i}^{p} + \boldsymbol{p}_p^{b} = \begin{bmatrix} r_p c\beta_i c\theta_y + z_0 s\theta_y \\ r_p c\beta_i s\theta_x s\theta_y + r_p s\beta_i c\theta_x - z_0 s\theta_x c\theta_y \\ -r_p c\beta_i c\theta_x s\theta_y + r_p s\beta_i s\theta_x + z_p + z_0 c\theta_x c\theta_y \end{bmatrix} \tag{3-3}$$

Where

$$\boldsymbol{p}_{\boldsymbol{p_i}}^{\boldsymbol{b}} = \begin{bmatrix} x_{p_i}^{b} & y_{p_i}^{b} & z_{p_i}^{b} \end{bmatrix}^T \quad \text{and} \quad \boldsymbol{p}_{\boldsymbol{p_i}}^{\boldsymbol{p}} = \begin{bmatrix} r_p c\beta_i & r_p s\beta_i & z_0 \end{bmatrix}^T$$

In Eq. (3-3), $\boldsymbol{Z_o}$ is the offset of the spherical joint with respect to coordinator system $\boldsymbol{O_p}$ and differentiate the Eq. (3-3) and get the result as follows:

$$\begin{bmatrix} \boldsymbol{\delta x}_{\boldsymbol{p_i}}^{\boldsymbol{b}} \\ \boldsymbol{\delta y}_{\boldsymbol{p_i}}^{\boldsymbol{b}} \\ \boldsymbol{\delta z}_{\boldsymbol{p_i}}^{\boldsymbol{b}} \end{bmatrix} = \begin{bmatrix} \boldsymbol{J_i} \end{bmatrix}_{3\times 6} \begin{bmatrix} \delta\theta_x \\ \delta\theta_y \\ \delta\theta_z \\ \delta x_p \\ \delta y_p \\ \delta z_p \end{bmatrix} \tag{3-4}$$

Where

$$\boldsymbol{J_i} = \begin{bmatrix} 0 & -r_p c\beta_i s\theta_y + z_0 c\theta_y & 0 & 0 & 0 & 0 \\ \left(r_p c\beta_i s\theta_y - z_0 c\theta_y\right) c\theta_x - r_p s\beta_i s\theta_x & \left(r_p c\beta_i c\theta_y + z_0 s\theta_y\right) s\theta_x & 0 & 0 & 0 & 0 \\ \left(r_p c\beta_i s\theta_y - z_0 c\theta_y\right) s\theta_x + r_p s\beta_i c\theta_x & -\left(r_p c\beta_i c\theta_y + z_0 s\theta_y\right) c\theta_x & 0 & 0 & 0 & 1 \end{bmatrix}_{3\times 6}$$

Since the active links have a fixed length, then it can be shown that

$$\left|\mathrm{O}_b\mathrm{P}_i - \mathrm{O}_b\mathrm{B}_i - \mathrm{B}_i\mathrm{D}_i\right| = \left|\mathrm{D}_i\mathrm{P}_i\right| \quad (i = 1,2,3) \tag{3-5}$$

Eq.(3-5) can be yielded

$$k_{i1}^2 + k_{i2}^2 + k_{i3}^2 = l_i^2 \tag{3-6}$$

Where

$$\begin{aligned} k_{i1} &= x_{p_i}^b - \left(r_b - u_i c\gamma\right) c\alpha_i \\ k_{i2} &= y_{p_i}^b - \left(r_b - u_i c\gamma\right) s\alpha_i \\ k_{i3} &= z_{p_i}^b - u_i s\gamma \end{aligned} \tag{3-7}$$

Here, γ represents the angle of the guide-way, and assuming there is only linear motion in the linear actuator of each active link, and the active link is a two-force component, only axial deformation occurs.

Then Eq. (3-6) can be differentiated as following:

$$\begin{bmatrix} \boldsymbol{\delta u_i} \\ \boldsymbol{\delta l_i} \end{bmatrix} = \begin{bmatrix} \frac{k_{i1}}{k_{i4}} & \frac{k_{i2}}{k_{i4}} & \frac{k_{i3}}{k_{i4}} \\ \frac{k_{i1}}{l_i} & \frac{k_{i2}}{l_i} & \frac{k_{i3}}{l_i} \end{bmatrix} \cdot \begin{bmatrix} \delta x_{p_i}^b \\ \delta y_{p_i}^b \\ \delta z_{p_i}^b \end{bmatrix} \quad (i = 1,2,3) \tag{3-8}$$

Where

$$k_{i4} = k_{i1} c\gamma c\alpha_i + k_{i2} c\gamma s\alpha_i - k_{i3} s\gamma$$

Substituting Eq. (3-4) into Eq. (3-8)

$$\begin{bmatrix} \delta u_1 \\ \delta u_2 \\ \delta u_3 \end{bmatrix} = \left(\boldsymbol{J}_t\right)_{3\times 6} \begin{bmatrix} \delta\theta_x \\ \delta\theta_y \\ \delta\theta_z \\ \delta x_p \\ \delta y_p \\ \delta z_p \end{bmatrix} = \begin{bmatrix} \left(\boldsymbol{J}_{t,1}\right)_{1\times 6} \\ \left(\boldsymbol{J}_{t,2}\right)_{1\times 6} \\ \left(\boldsymbol{J}_{t,3}\right)_{1\times 6} \end{bmatrix} \begin{bmatrix} \delta\theta_x \\ \delta\theta_y \\ \delta\theta_z \\ \delta x_p \\ \delta y_p \\ \delta z_p \end{bmatrix}$$

The twist of the platform can be defined as

$$\mathbf{t} = \begin{bmatrix} \boldsymbol{\omega}^T & \dot{\mathbf{p}}^T \end{bmatrix}^T = \begin{bmatrix} \delta\theta_x & \delta\theta_y & \delta\theta_z & \delta x_p & \delta y_p & \delta z_p \end{bmatrix}^T \tag{3-9}$$

Here, we have

$$\dot{\boldsymbol{\rho}} = \mathbf{J}\mathbf{t} = \begin{bmatrix} \delta l_1 & \delta l_2 & \delta l_3 \end{bmatrix}^T \tag{3-10}$$

$$\begin{bmatrix} \delta l_1 \\ \delta l_2 \\ \delta l_3 \end{bmatrix} = \left(\boldsymbol{J}_p\right)_{3\times 6} \begin{bmatrix} \delta\theta_x \\ \delta\theta_y \\ \delta\theta_z \\ \delta x_p \\ \delta y_p \\ \delta z_p \end{bmatrix} = \begin{bmatrix} \left(\boldsymbol{J}_{p,1}\right)_{1\times 6} \\ \left(\boldsymbol{J}_{p,2}\right)_{1\times 6} \\ \left(\boldsymbol{J}_{p,3}\right)_{1\times 6} \end{bmatrix} \begin{bmatrix} \delta\theta_x \\ \delta\theta_y \\ \delta\theta_z \\ \delta x_p \\ \delta y_p \\ \delta z_p \end{bmatrix} \tag{3-11}$$

Where

$$\boldsymbol{J_p} = \begin{bmatrix} \frac{k_{i1}}{l_i} & \frac{k_{i2}}{l_i} & \frac{k_{i3}}{l_i} \end{bmatrix} \cdot \boldsymbol{J_i} \qquad (3\text{-}12)$$

3.3 Forward Kinematics

The direct kinematics problem will solve the pose of the end-effectors $\boldsymbol{T_p^b}$ when the joint motion$\boldsymbol{u_i}$ $(\boldsymbol{i = 1, 2, 3},)$ is known. The solution of direct kinematic problem can also be derived from Eq. (3-3). Currently the motions of the end effectors $(\boldsymbol{\theta_x, \theta_y, Z_p})$ are unknown and the joint motion $\boldsymbol{u_i}$ $(\boldsymbol{i = 1, 2, 3},)$ is given. To solve the direct kinematic problem, $\boldsymbol{Z_p}$ and $\boldsymbol{\theta_y}$ could be represented by $\boldsymbol{\theta_x}$

Therefore, Eq. (3-13) can be deduced from Eqs. (3-6) and (3-7)

$$z_p^2 + \left(A_i s\theta_y + B_i\right) z_p + \left(C_i c\theta_y + D_i s\theta_y + E_i\right) = 0 \qquad (i = 1, 2, 3) \qquad (3\text{-}13)$$

As shown the coefficients $A_i \sim E_i$ are the following functions of $\boldsymbol{\theta_x}$,

$$A_i = -2r_p c\beta_i c\theta_x$$

$$B_i = 2\left(r_p s\beta_i s\theta_x - u_i s\gamma\right)$$

$$C_i = -2\left(r_b - u_i c\gamma\right) r_p c\alpha_i c\beta_i \tag{3-14}$$

$$D_i = 2r_p c\beta_i \left(u_i s\gamma c\theta_x - \left(r_b - u_i c\gamma\right) s\alpha_i s\theta_x\right)$$

$$E_i = r_p^2 + r_b^2 + u_i^2 - l_i^2 - 2\left(r_p s\beta_i \left(u_i s\gamma s\theta_x + \left(r_b - u_i c\gamma\right) s\alpha_i c\theta_x\right) + r_b u_i c\gamma\right)$$

From Eq. (3-13)

$$C\theta_y = -\frac{Fz_p^2 + Gz_p + H}{Kz_p + L} \tag{3-15}$$

$$S\theta_y = -\frac{Iz_p + J}{Kz_p + L} \tag{3-16}$$

Where the coefficients $\boldsymbol{F \sim L}$ are functions of $\boldsymbol{\theta_x}$, expressed by

$$F = B_{12}A_{13} - B_{13}A_{12}$$

$$G = E_{12}A_{13} + B_{12}D_{13} - E_{13}A_{12} - B_{13}D_{12}$$

$$H = E_{12}D_{13} - E_{13}D_{12}$$

$$I = C_{12}B_{13} - C_{13}B_{12} \tag{3-17}$$

$$J = C_{12}E_{13} - C_{13}E_{12}$$

$$K = C_{12}A_{13} - C_{13}A_{12}$$

$$L = C_{12}D_{13} - C_{13}D_{12}$$

And

$$A_{ij} = A_i - A_j, B_{ij} = B_i - B_j, C_{ij} = C_i - C_j$$
$$D_{ij} = D_i - D_j, E_{ij} = E_i - E_j \tag{3-18}$$

Since $\cos^2\theta_y + \sin^2\theta_y = 1$ substitute Eq. (3-15) and Eq. (3-16) into this expression, yields

$$M_4 z_p^4 + M_3 z_p^3 + M_2 z_p^2 + M_1 z_p + M_0 = 0 \tag{3-19}$$

Where:

$$M_4 = F^2$$
$$M_3 = 2FG$$
$$M_2 = G^2 + I^2 + K^2 + 2FH$$
$$M_1 = z_e^2 + 2\left(GH + IJ + KL\right)$$
$$M_0 = H^2 + J^2 + L^2$$

It can be observed that Eq. (3-13) includes three independent equations. Thus, two independent equations Eqs. (3-15) and (3-16), have been derived. The other one can be derived by substituting Eqs. (3-15) and (3-16) into any items in Eq. (3-6). For example, the equation when ***i*** = *1* is

$$N_3 z_p^3 + N_2 z_p^2 + N_1 z_p + N_0 = 0 \tag{3-20}$$

Where

$$
\begin{aligned}
N_3 &= K \\
N_2 &= B_1K + L - A_1I - C_1F \\
N_1 &= E_1K + B_1L - A_1J - D_1I - C_1G \\
N_0 &= E_1L - D_1J - C_1H
\end{aligned}
\tag{3-21}
$$

The direct kinematic problem is solved for the given design, then Eqs. (3-19) and (3-20) should possess a common solution of $\boldsymbol{Z_p}$. Based on Bezout's method, the following condition should be satisfied:

$$
\begin{vmatrix}
M_4 & M_3 & M_2 & M_1 & M_0 & 0 & 0 \\
0 & M_4 & M_3 & M_2 & M_1 & M_0 & 0 \\
0 & 0 & M_4 & M_3 & M_2 & M_1 & M_0 \\
N_3 & N_2 & N_1 & N_0 & 0 & 0 & 0 \\
0 & N_3 & N_2 & N_1 & N_0 & 0 & 0 \\
0 & 0 & N_3 & N_2 & N_1 & N_0 & 0 \\
0 & 0 & 0 & N_3 & N_2 & N_1 & N_0
\end{vmatrix} = 0
\tag{3-22}
$$

Eq. (3-22) becomes an equation for $\boldsymbol{\theta_x}$ when the joint motion $\boldsymbol{u_i}$ is given. If Eq. (3-22) is converted using the standard transformation formula,

$$
C\theta_x = \left(1 - t^2\right) / \left(1 + t^2\right), S\theta_x = 2t / \left(1 + t^2\right), \left(t = \tan\left(\theta_x / 2\right)\right)
$$

Then it is a polynomial equation with an order of 40.

After $\boldsymbol{\theta_x}$ is obtained from Eq. (3-22), $\boldsymbol{Z_p}$ and $\boldsymbol{\theta_y}$ can be calculated sequentially from Eqs. (3-19), (3-20) and Eqs. (3-15) and (3-16)**.**

3.4 Jacobian Matrix

Each of the kinematic chains connecting the base to the platform can be taken as a serial mechanism and a Hooke joint can be replaced by two orthogonal revolute joints in the present study.

Presented in Figures 2.4 and 2.5, this three-degree-of-freedom mechanism consists of four kinematic chains, including three variable length legs with identical topology and one passive constraining leg, connecting the base to a moving platform. In this 3-DOF parallel mechanism, the kinematic chains associated with the three identical legs (links) are connected to the base platform with a universal joint, an actuated prismatic joint and a spherical joint attached to the moving platform. The fourth chain connecting the fixed base center to the moving platform center is a passive constraining leg and has a different architecture from the other three identical chains. It consists of a prismatic joint attached to the fixed base and a universal joint attached to the moving platform. This last leg is used to constrain the motion of the platform to only three degrees of freedom.

The parallel mechanism we studied comprises two main components, namely, the constraining leg which can be thought of as a serial mechanism and the actuated legs acting in parallel.

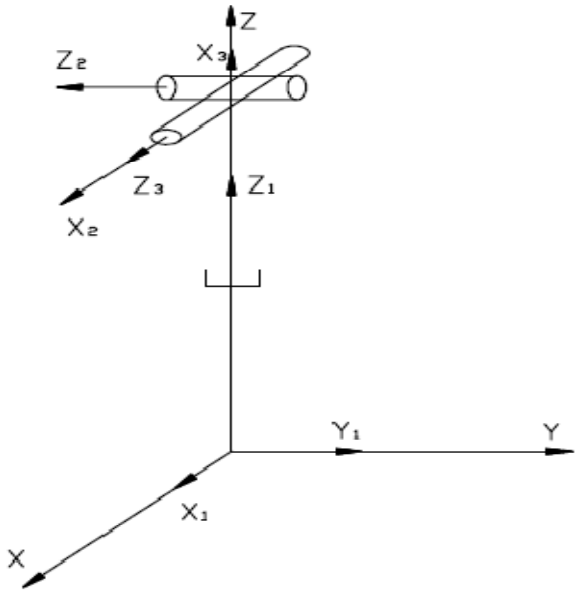

Figure 3.2 D-H Coordinate Frames for the Passive Constraining Leg [19]

Since the passive constraining leg is a 3-DOF open loop chain, its posture can be completely described by three joint variables, and they can be denoted as θ_x, θ_y and Z, Note that the universal joint is equivalent to two intersecting revolute joints.

Figure 3.2 illustrates the configuration of the passive leg, from Figure 3.2 we can obtain the Denavit-Hartenberg (DH) parameters table as shown in Table1

i	a_i	b_i	α_i	θ_i
0	0	0	0	0
1	0	Z	90°	0
2	0	0	90°	θ_x
3	0	0	0	θ_y

Table 1: DH Parameters for the Passive Constraining Leg of 3-DOF Mechanism

Considering the passive constraining leg, for 3-DOF mechanism we can write

$$\mathbf{J}_{n+1}\dot{\boldsymbol{\theta}}_{n+1} = \mathbf{t}, \quad n = 3 \tag{3-23}$$

Where $\boldsymbol{t} = \left[\boldsymbol{\omega}^T \dot{\boldsymbol{P}}^T\right]^T$ is the twist of the platform, with ω the angular velocity of the platform and

$$\dot{\theta}_{n+1} = \left[\dot{\theta}_{n+1,1} \cdots \dot{\theta}_{n+1,n}\right] \tag{3-24}$$

is the joint velocity vector associated with the constraining leg. Matrix J_{n+1} is the Jacobian matrix of the constraining leg considered as a serial n-DOF mechanism, which can be expressed as (Angeles 1997)

$$\mathbf{J}_{n+1} = \left[\begin{array}{c|c} \mathbf{e}_{n+1,1} & \cdots \quad \mathbf{e}_{n+1,n} \\ \mathbf{e}_{n+1,n} \times \boldsymbol{r}_{n+1,n} & \cdots \quad \mathbf{e}_{n+1,n} \times \boldsymbol{r}_{n+1,n} \end{array}\right] \quad n = 3 \tag{3-25}$$

Here $\mathbf{r}_i$ is the vector connecting the origin of frame b_i to the origin of the platform frame. It is important to note that if the $\boldsymbol{i_{th}}$ pair is a revolute joint, then the $\boldsymbol{i_{th+1}}$ column of J_{n+1}, noted j_i, can be written as

$$\mathbf{J}_i = \begin{bmatrix} \mathbf{e}_i \\ \mathbf{e}_i \times r_i \end{bmatrix} \tag{3-26}$$

On the other hand, if the $\boldsymbol{i_{th}}$ pair is a prismatic joint, then the $(\boldsymbol{i-1})_{\boldsymbol{th}}$ and the $\boldsymbol{i_{th}}$ links have the same angular velocity, for a prismatic joint does not have any rotation, then the $\boldsymbol{i_{th}}$ column of $\boldsymbol{J_{n+1}}$ changes to

$$\mathbf{J}_i = \begin{bmatrix} 0 \\ \mathbf{e}_i \times r_i \end{bmatrix} \tag{3-27}$$

Here if we take base frame as frame 0, and defined $a_0 = 0, \theta_0 = 0$, and then

$$\boldsymbol{Q}_{40} = \boldsymbol{1} \tag{3-28}$$

Where Q_{40} is the rotation matrix from the fixed reference (base-platform) to the passive leg and then we have

$$\boldsymbol{e}_{41} = \boldsymbol{Q}_{40}\boldsymbol{e}_{40} \tag{3-29}$$

$$\boldsymbol{e}_{41} = \boldsymbol{Q}_{40}\boldsymbol{Q}_{41}\boldsymbol{e}_{40} \tag{3-30}$$

$$\boldsymbol{e}_{42} = \boldsymbol{Q}_{40}\boldsymbol{Q}_{41}\boldsymbol{Q}_{42}\boldsymbol{e}_{40} \tag{3-31}$$

And the position vectors can be expressed as following

$$\boldsymbol{r}_{41} = \boldsymbol{Q}_{40}\boldsymbol{a}_{41} + \boldsymbol{Q}_{40}\boldsymbol{Q}_{41}\boldsymbol{a}_{42} + \boldsymbol{Q}_{40}\boldsymbol{Q}_{41}\boldsymbol{Q}_{42}\boldsymbol{a}_{43} \tag{3-32}$$

$$\boldsymbol{r}_{42} = \boldsymbol{Q}_{40}\boldsymbol{Q}_{41}\boldsymbol{a}_{42} + \boldsymbol{Q}_{40}\boldsymbol{Q}_{41}\boldsymbol{Q}_{42}\boldsymbol{a}_{43} \tag{3-33}$$

$$\boldsymbol{r}_{43} = \boldsymbol{Q}_{40}\boldsymbol{Q}_{41}\boldsymbol{Q}_{42}\boldsymbol{a}_{43} \tag{3-34}$$

The velocity equation of the fourth kinematic chain (passive leg) is

$$J_4\dot{\theta}_4 = \boldsymbol{t} \tag{3-35}$$

And here

$$\dot{\boldsymbol{\theta}}_4 = \begin{bmatrix} \dot{\boldsymbol{\rho}} & \dot{\boldsymbol{\theta}}_x & \dot{\boldsymbol{\theta}}_y \end{bmatrix} \tag{3-36}$$

And the Jacobian matrix of the passive leg can be expressed as

$$J_4 = \begin{bmatrix} 0 & e_{42} & e_{43} \\ e_{41} & e_{42}\times r_{42} & e_{43}\times r_{43} \end{bmatrix} \tag{3-37}$$

If we defined Jacobian as a 6×3 matrix shown below:

$$J_4 = \begin{bmatrix} \mathbf{A} \\ \mathbf{B} \end{bmatrix} \tag{3-38}$$

So **A** and **B** are denoted as the 3×3 matrix defined as

$$\mathbf{A} = \begin{bmatrix} \boldsymbol{0} & \boldsymbol{e}_{42} & \boldsymbol{e}_{43} \end{bmatrix} \tag{3-39}$$

$$\mathbf{B} = \begin{bmatrix} \boldsymbol{e}_{41} & \boldsymbol{e}_{42}\times\boldsymbol{r}_{42} & \boldsymbol{e}_{43}\times\boldsymbol{r}_{43} \end{bmatrix} \tag{3-40}$$

Finally we get the Jacobin of passive leg as following

$$\boldsymbol{J_4} = \begin{bmatrix} 0 & 0 & \sin(\theta_x) \\ 0 & -1 & 0 \\ 0 & 0 & -\cos(\theta_x) \\ 0 & 0 & 0 \\ 0 & 0 & 0 \\ 1 & 0 & 0 \end{bmatrix} \tag{3-41}$$

According to the principle of virtual work, we have

$$\boldsymbol{\tau}^T \dot{\boldsymbol{\rho}} = \mathbf{w}^T \mathbf{t} \tag{3-42}$$

Here $\boldsymbol{\tau}$ is a vector of the actuator forces applied at each joint and w is the wrench, which is the torque and force, applied to the moving platform. It is assumed that no gravitational forces act on any of the intermediate links. Consequently, we have $\boldsymbol{W} = [\mathbf{n}^T \quad \mathbf{f}^T]^T$ where $\mathbf{n}$ and $\mathbf{f}$ are respectively the external torque and force applied to the platform.

Rearranging Eq. (3-9) and substituting it into Eq. (3-42), we obtain

$$\boldsymbol{\tau}^T \mathbf{J}_P \mathbf{t} = \mathbf{w}^T \mathbf{t} \tag{3-43}$$

Now, substituting Eq. (3-35) into Eq. (3-43), we have

$$\boldsymbol{\tau}^T \mathbf{J}_p \mathbf{J}_4 \dot{\boldsymbol{\theta}}_4 = \mathbf{w}^T \mathbf{J}_4 \dot{\boldsymbol{\theta}}_4 \tag{3-44}$$

The latter equation must be satisfied for the arbitrary values of $\dot{\boldsymbol{\theta}}_4$ and hence, we can write

$$\left(\mathbf{J}_p \mathbf{J}_4\right)^T \tau = \mathbf{J}_4^T \mathbf{W} \tag{3-45}$$

The latter equation relates the actuator forces, which are applied to the end-effector in static mode, to the Cartesian wrench **w**. Since all links are assumed to be rigid, the compliance of the mechanism will be induced solely by the compliance of the actuators. An actuator compliance matrix, **C,** is therefore defined as

$$\mathbf{C}\ \boldsymbol{\tau}\ =\ \Delta\ \boldsymbol{\rho} \tag{3-46}$$

Where $\boldsymbol{\tau}$ is the vector of the actuated joint forces and $\Delta\boldsymbol{\rho}$ is the induced joint displacement. Matrix C is a (3x3) diagonal matrix whose $\boldsymbol{i_{th}}$ diagonal entry represents the compliance of the $\boldsymbol{i_{th}}$ actuator.

Now, Eq. (3-43) can be rewritten as

$$\boldsymbol{\tau}\ =\ (\mathbf{J}_{p}\mathbf{J}_{4})^{-T}\,\mathbf{J}^{T}{}_{4}\mathbf{W} \tag{3-47}$$

The substitution of Eq. (3-47) into Eq. (3-46) then leads to

$$\Delta\boldsymbol{\rho}\ =\ \mathbf{C}\,(\mathbf{J}_{p}\mathbf{J}_{4})^{-T}\,\mathbf{J}^{T}{}_{4}\mathbf{W} \tag{3-48}$$

Moreover, for a vector representing minor displacement, $\Delta\boldsymbol{\rho}$, Eq. (3-48)can be written as

$$\Delta\ \boldsymbol{\rho}\ \cong\ \mathbf{J}\ \Delta\ \mathbf{c} \tag{3-49}$$

Where ΔC is a vector representing small Cartesian displacement and rotation, is defined as

$$\Delta\ \mathbf{c}\ =\ \left[\ \Delta\ \mathbf{p}^{\ T}\qquad \Delta\ \boldsymbol{\alpha}^{\ T}\ \right]^{T} \tag{3-50}$$

Here, $\Delta\ \boldsymbol{\alpha}$ is the change of orientation,

$$\Delta \boldsymbol{\alpha} = vect(\Delta \mathbf{Q}\, \mathbf{Q}^T) \tag{3-51}$$

Here ΔQ is the variation of the orientation and $vect(\Delta QQ^T)$ is the linear invariant vector of its matrix.

Similarly, for small displacements, Eq. (3-35) can also be written, as

$$\mathbf{J}_4 \Delta \boldsymbol{\theta}_4 \cong \Delta \mathbf{c} \tag{3-52}$$

Here $\Delta \boldsymbol{\theta}_4$ is a vector representing minor variations of the passive leg's joint coordinates.

Substituting Eq. (3-49) into Eq. (3-48),

$$\mathbf{J}_p \Delta \mathbf{c} = \mathbf{C}(\mathbf{J}_p \mathbf{J}_4)^{-T} \mathbf{J}^T{}_4 \mathbf{W} \tag{3-53}$$

Substituting Eq. (3-52) into Eq. (3-53),

$$\mathbf{J}_p \mathbf{J}_4 \Delta \boldsymbol{\theta}_4 = \mathbf{C}(\mathbf{J}_p \mathbf{J}_4)^{-T} \mathbf{J}^T{}_4 \mathbf{W} \tag{3-54}$$

Then, multiplying both sides of Eq. (3-54) by $(\mathbf{J}\mathbf{J}_4)^{-1}$,

$$\Delta \boldsymbol{\theta}_4 = (\mathbf{J}_p \mathbf{J}_4)^{-1} \mathbf{C} (\mathbf{J}_p \mathbf{J}_4)^{-T} \mathbf{J}_4{}^T \mathbf{W} \tag{3-55}$$

and finally, multiplying both sides of Eq. (3-55) by $\mathbf{J}_4$,

$$\Delta \mathbf{c} = \mathbf{J}_4 (\mathbf{J}_p \mathbf{J}_4)^{-1} \mathbf{C} (\mathbf{J}_p \mathbf{J}_4)^{-T} \mathbf{J}^T{}_4 \mathbf{W} \tag{3-56}$$

Hence, the Cartesian compliance matrix becomes

$$\mathbf{C}_c = \mathbf{J}_4 (\mathbf{J}_p \mathbf{J}_4)^{-1} \mathbf{C} (\mathbf{J}_p \mathbf{J}_4)^{-T} \mathbf{J}_4^T \tag{3-57}$$

with

$$\Delta \mathbf{c} = \mathbf{C}_c \mathbf{w} \tag{3-58}$$

Here $\mathbf{C}_c$ is a symmetrical, positive, semi-definite (6x6) matrix, as expected.

3.5 Stiffness Modeling

Stiffness is one of the most important consideration facts in the design of parallel kinematic manipulator. After we get the stiffness result of the structure, the next step is design optimization. The stiffness of a parallel kinematic manipulator is given by its system stiffness matrix. As in the stiffness model of this PKM, we consider the structure frames and the links are rigid bodies, so the Cartesian stiffness matrix $\boldsymbol{K_c}$ is opposite the Cartesian compliance matrix $\mathbf{C}_c$. So from the Eq. (3-57) we got following:

$$\boldsymbol{K_c} = \mathbf{C}_c{}^{-1} = \left[\mathbf{J}_4 (\mathbf{J}_p \mathbf{J}_4)^{-1} \mathbf{C} (\mathbf{J}_p \mathbf{J}_4)^{-T} \mathbf{J}_4^T \right]^{-1}$$

In this case we fixed the moving platform in certain angle in x –axis, and use the design kinematic parameter which shown in Table 2. We got stiffness map in following figures;

α_i	$[-30^\circ \quad 90^\circ \quad 150^\circ]$	$i = 1,2,3$
β_i	$[-30^\circ \quad 90^\circ \quad 150^\circ]$	$i = 1,2,3$
r_b	50 mm	
r_a	25 mm	
l_i	120 mm	$i = 1,2,3$
γ	50°	
Spherical Joint	$\{-40^\circ \ to \ 40^\circ\}$	
Universal Joint	$\{-50^\circ \ to \ 50^\circ\}$	
Prismatic Joint (Passive Link)	50 mm	

Table 2 Three Action Legs Kinematic Parameters

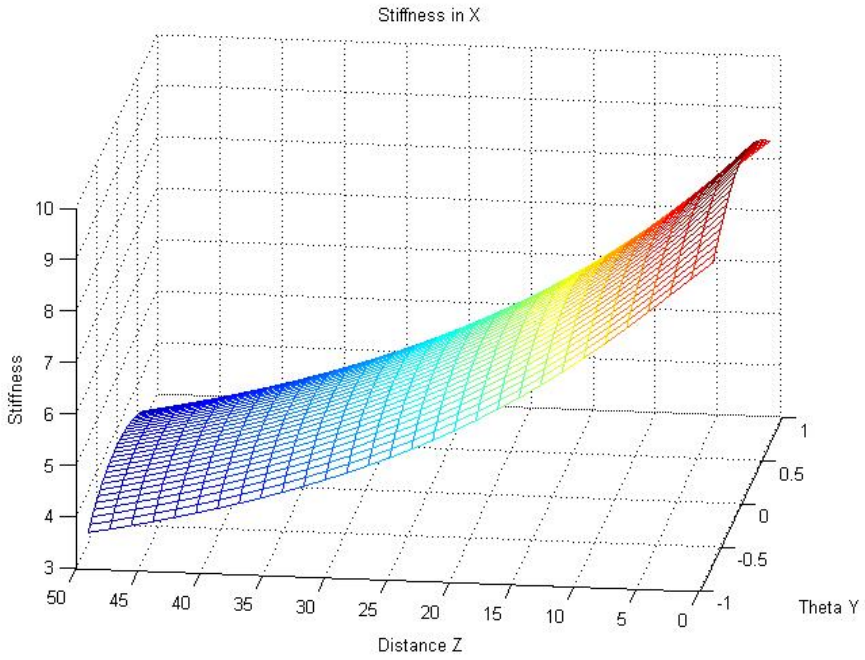

Figure 3.3 Stiffness in X axis (a)

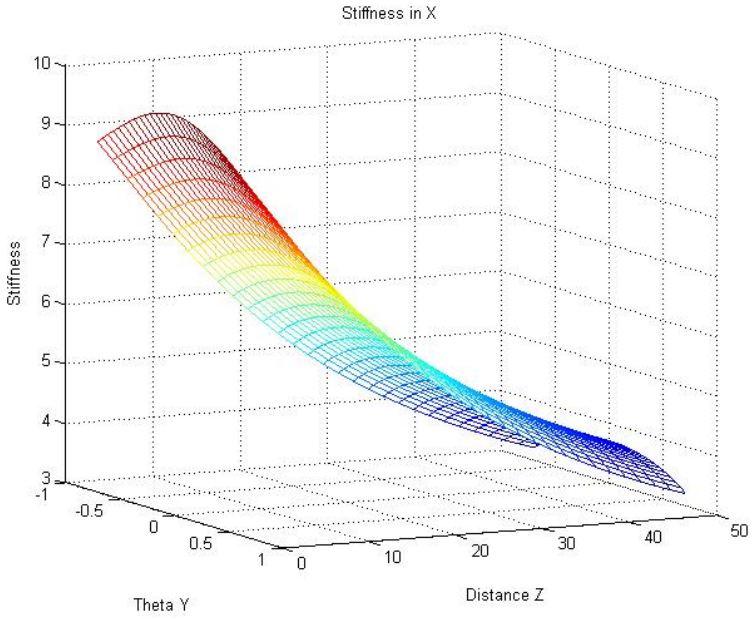

Figure 3.4 Stiffness in X axis (b)

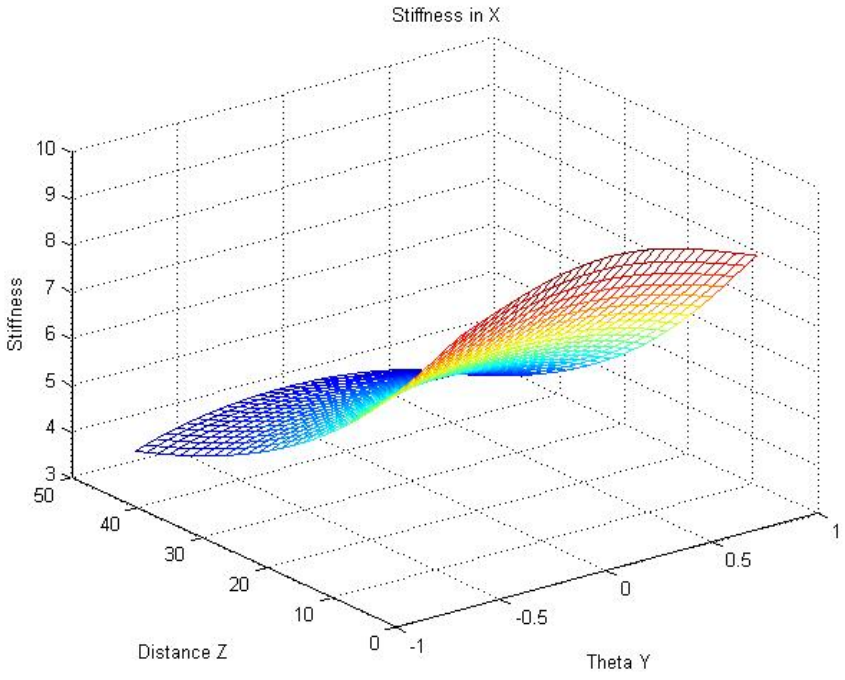

Figure 3.5 Stiffness in X axis (c)

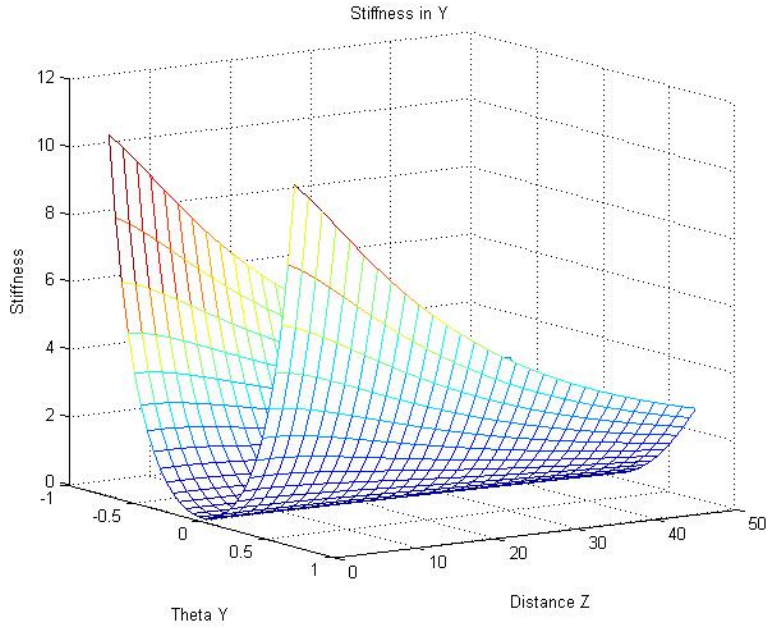

Figure 3.6 Stiffness in Y axis (a)

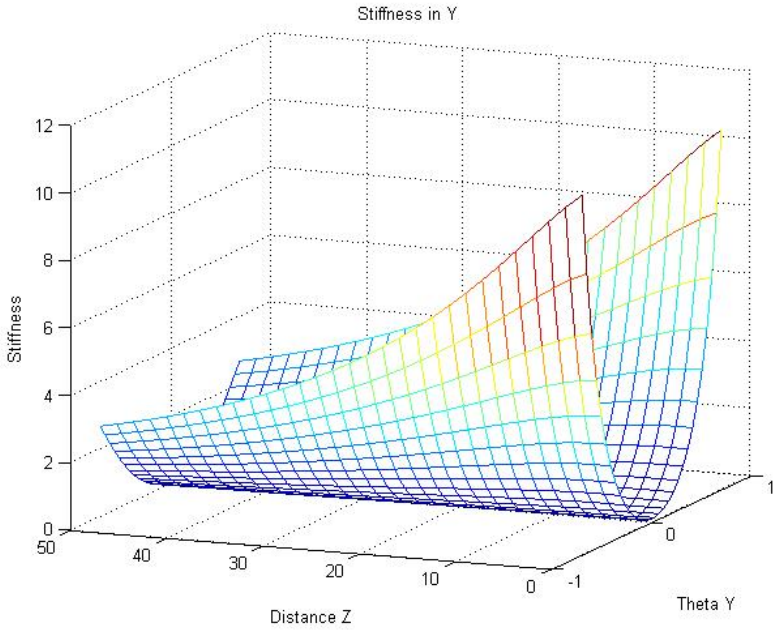

Figure 3.7 Stiffness in Y axis (b)

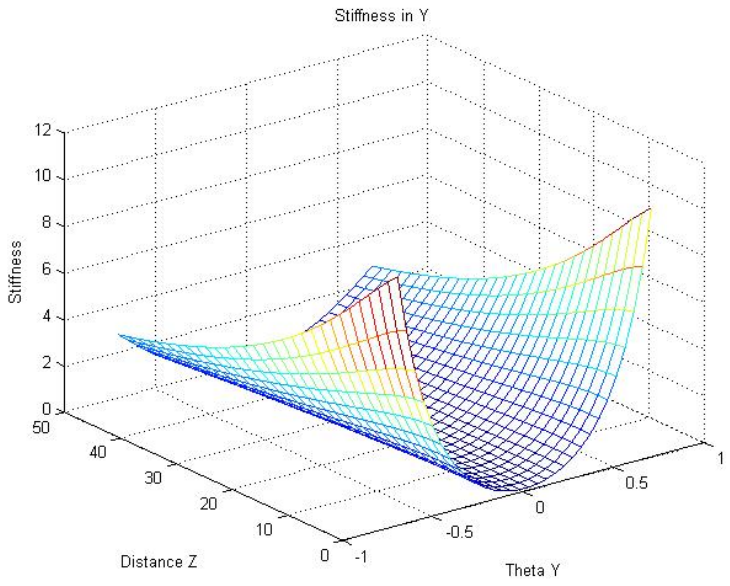

Figure 3.8 Stiffness in Y axis (c)

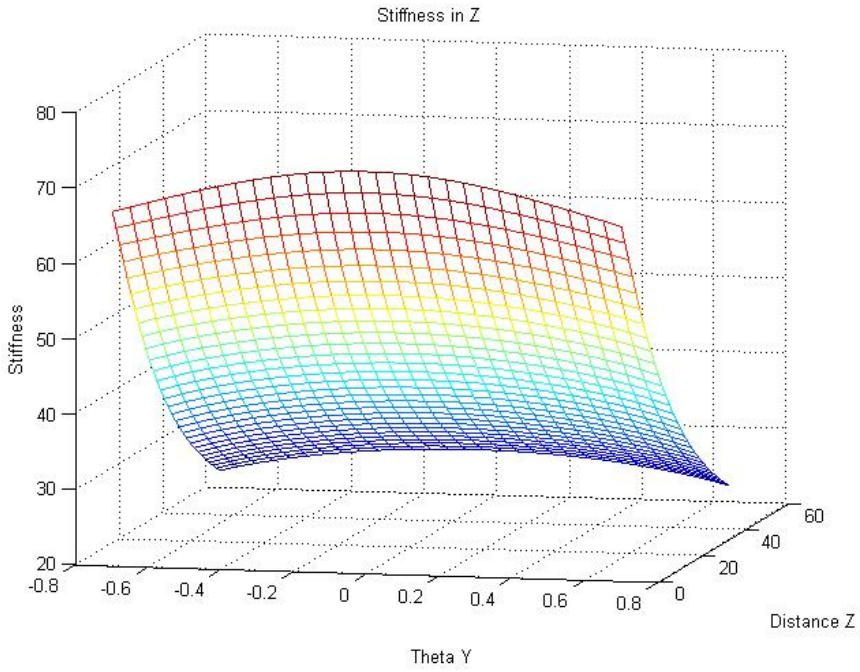

Figure 3.9 Stiffness in Z axis (a)

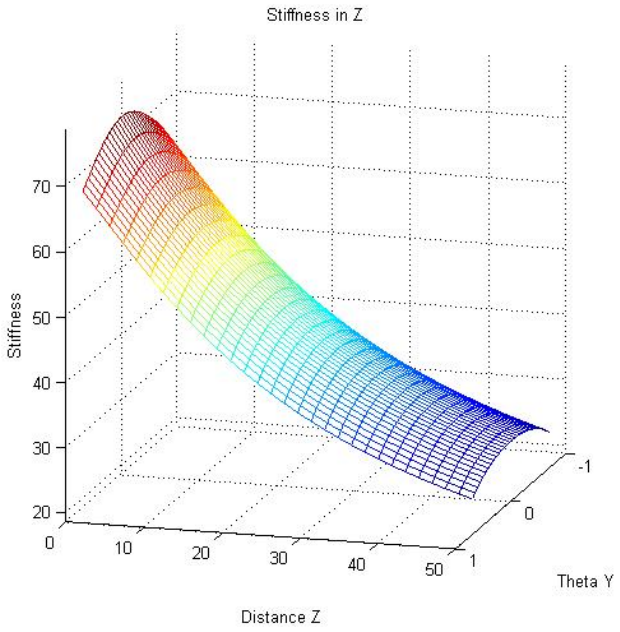

Figure 3.10 Stiffness in Z axis (b)

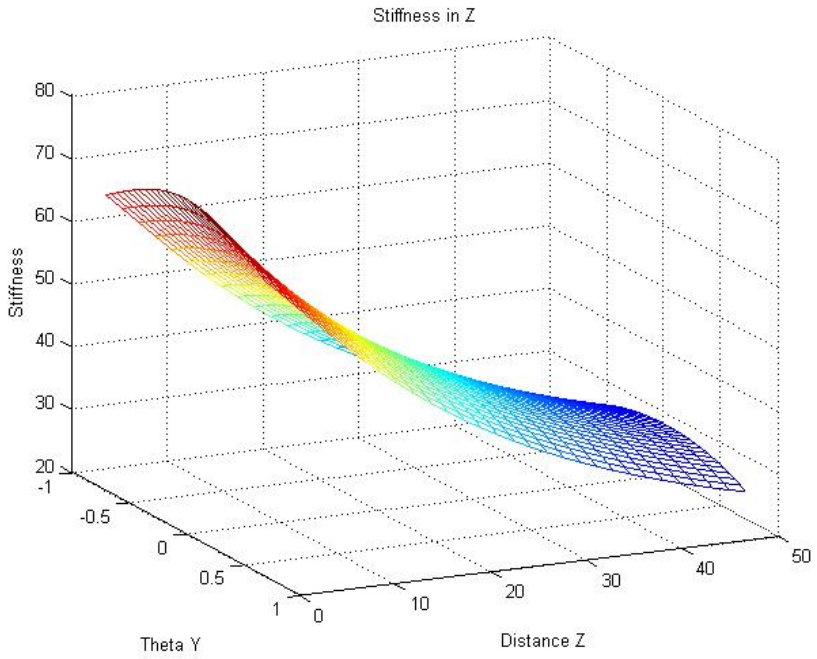

Figure 3.11 Stiffness in Z axis (c)

3.6 Conclusion

From above stiffness mesh graphs, Figure 3.3 to Figure 3.5 show the stiffness in X axis with different view angle, same as Figure 3.6 to Figure 3.8 shows the stiffness in Y axis. Figure 3.9, Figure 3.10 and Figure 3.11 shows the stiffness in Z axis. For stiffness in X axis, one can conclude that stiffness is decreased when the magnitude of Z coordinates increase, and also stiffness is symmetrical along the Y axis. For stiffness in Y axis, it reaches the maximum values at absolute $|Y|=1$ point, and has symmetry along Y axis. Also the maximum points are located at Z coordinate's small value point. For the stiffness in Z axis, the main change of the stiffness is along with Z coordinate, there is not much change when X and Y value change.

This parallel kinematic manipulator (PKM) with three active kinematic chains and a passive leg has improved precision and stiffness maps by:

- Providing drive and actuation of each active kinematic chain by devices secured rigidly to a support structure so that only a fixed length leg of the chain is suspended.
- Driving the fixed length leg of the active kinematic chain to move in a direction oblique to a direction of the fixed length leg.

- Providing a prismatic jointed leg that is rigidly secured to the base structure and coupled by an effectively universal joint to the motion platform.

Chapter 4

Kinematic Modeling of 3-DOF Micro Motion Manipulator with Actuation Redundancy

4.1 CAD Modeling of the 3-DOF Micro Motion Manipulator with Actuation Redundancy

The word redundant is commonly used to mean "exceeding what is necessary or normal", or extra what they needs. There are mainly two different types of redundancy for parallel manipulators: a) kinematic redundancy and b) actuation redundancy. A parallel manipulator is to be said to be kinematic redundant manipulator when mobility of the mechanism is greater than the required degrees of freedom of the moving platform. On the other hand, a parallel manipulator is called redundantly actuated manipulator when the number of actuators is great than the mobility of the mechanism. It is believed that redundancy can improve the ability and the performance of parallel manipulator [27] and

[28]. The reason we used the redundant mechanisms is that it can solve the singularity problem, and improve the stiffness of the structure.

In the chapter 3 we have solved the kinematic problem of 3-DOF micro motion parallel manipulator. In this chapter, we will follow the same procedure, and go on to discuss parallel manipulator which has actuation redundancy. Normally actuation redundancy is only applied to the closed-link mechanisms. However, singularity is a common problem in parallel mechanisms. We will show that the behavior of singularity of parallel mechanisms can be more complicated than that of serial ones. However, it is not clear whether singularity will bring problems to kinematics, dynamics or other characteristics and what the result will be when parallel mechanisms fall into the neighborhood of a singularity. Thus, we propose that the greatest advantage of actuation redundancy is avoiding the singularity of the parallel manipulator and increasing the stiffness of the structure.

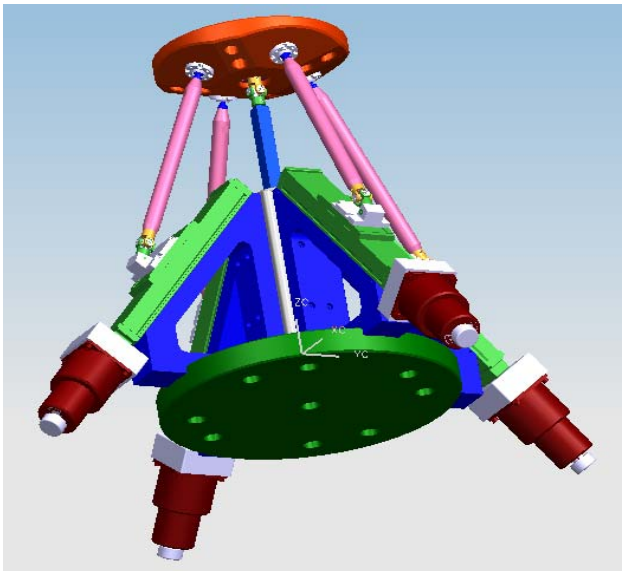

Figure 4.1 3-DOF Micro Motion Manipulator with Actuation Redundancy

Compared with the 3-DOF parallel manipulator with passive leg, the architecture of 3-DOF redundant actuator parallel manipulator with passive leg is shown in Figure. 4.1. This manipulator is composed of a moving plate, a fixed base, 4 limb links with identical kinematic structures and 1 passive limb. The 4 limb links are arranged in 90 degree intervals on the guide way and are connected with the driving block by a universal joint and a spherical joint attached to the moving plate. A linear actuator drives each prismatic joint. The 5^{th} leg (middle leg) connects the fixed base to the moving plate by a prismatic joint followed by a universal joint. The connectivity of the 5^{th} leg is equal to three. Therefore, it provides three constraints on the moving plate. We called the 5^{th} leg a passive leg because it is not driven by any actuator.

As shown in Figure 4-1, this parallel manipulator include the universal joint of the passive link, located on the moving platform rather than the base platform, so the motions along *x* and *y* translations and *Z* rotation are eliminated.

As in the previous chapter, the reference point on the moving platform has uncoupled motion with *X* and *Y* rotations and *Z* translation. The proposed manipulator has three platforms: base platform $B_1B_2B_3B_4$, middle platform $m_1m_2m_3m_4$, and moving platform$P_1P_2P_3P_4$. The base platform is fixed on the ground. The middle platform is used to support guide-way B_im_i of actuated links D_iP_i .The moving platform is used to mount a tool. The passive link is installed between the middle platform and the moving platform. Actuated links D_iP_i are connected to the moving platform by a spherical joint (ball joint) at P_i, and to a slider connected to the active ball screw by a universal joint at D_i. The passive link with a prismatic joint is fixed on the middle platform at one end, and connected to the end-effector platform by a universal joint at the other end.

Following parameters define other details of the structure:

- The angle α_i (i =1,2,3,4) between X_b and O_bB_i ,
- The angle β_i (i=1,2,3,4) between X_p and O_pP_i ,
- The distance from $O_b\ to\ B_i$ on the base platform is r_b,

- The distance from O_p *to* P_i *at* the end-effector platform is r_p ,
- The angle of a guide-way $\boldsymbol{\gamma}$,
- The length of an active link $\boldsymbol{l_i}$, and
- The offset of the spherical joints on the platform $\boldsymbol{Z_o}$.

As shown in Figure 4.2, we also use same two coordinate systems, $\{O_p - X_pY_pZ_p\}$ and $\{O_b - X_bY_bZ_b\}$, which are attached to the end-effector and base platform, respectively. For the origin O_p of the end-effector, its translational motions along X_p and Y_p, and rotational motion along Z_p, are eliminated because of the usage of the passive leg.

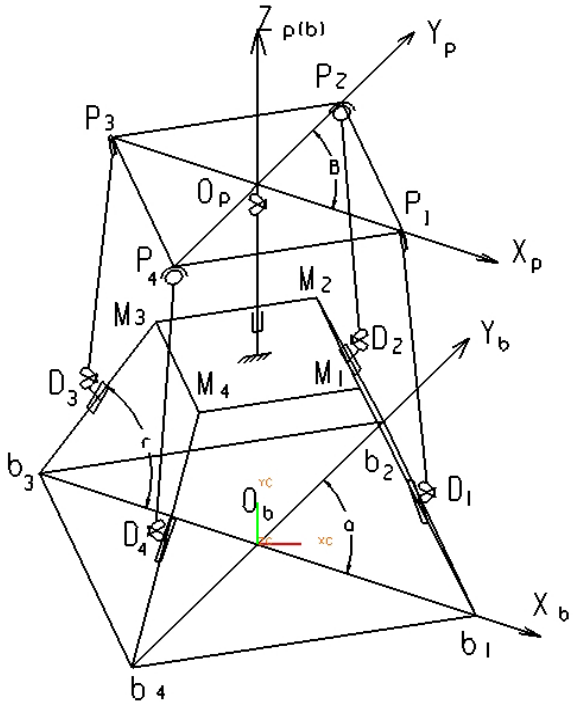

Figure 4.2 Schematic of 3-DOF Micro Motion Manipulator with Actuation Redundancy

4.2 Inverse Kinematics

The position vector of points of $\boldsymbol{P_i}$ and $\boldsymbol{B_i}$ with respect to the coordinate frames P and b, respectively, can be written as

$$\begin{aligned} \boldsymbol{P_{pi}} &= \left[r_a \cos\beta_i, \quad r_a \sin\beta_i, \quad 0 \right]^T, \qquad i = 1,2,3,4 \\ \boldsymbol{B_{bi}} &= \left[r_b \cos\beta_i, \quad r_b \sin\beta_i, \quad 0 \right]^T, \qquad i = 1,2,3,4 \end{aligned} \tag{4-1}$$

Where r_a and r_b are the length of the $\overline{O\,P_i}$ and $\overline{O'B_i}$, respectively, angle β_i is measured from the x axis to the line $O\,P_i$ and is equal to the x axis to the line $O'B_i$, $\beta_i =$ $0^\circ, 90^\circ, 180^\circ, 270^\circ$ ($i = 1,2,3,4$).

To facilitate the analysis, a position vector, $\boldsymbol{P_B}$ is used to define the position of the moving platform,

$$\boldsymbol{P_B} = \left[p_x, p_y, p_z \right]^T \tag{4-2}$$

And a rotation matrix, $\boldsymbol{R_B^P}$, is used to define the orientation of the moving platform with respect to the fixed base,

$$\boldsymbol{R}_{\boldsymbol{B}}^{\boldsymbol{P}} = R_Z(\phi)R_Y(\theta)R_X(\psi)$$

$$= \begin{bmatrix} \cos\phi\cos\theta & \cos\phi\sin\theta\sin\psi - \sin\phi\cos\psi & \cos\phi\sin\theta\cos\psi - \sin\phi\sin\psi \\ \sin\phi\cos\theta & \sin\phi\sin\theta\sin\psi - \cos\phi\cos\psi & \sin\phi\sin\theta\cos\psi - \cos\phi\sin\psi \\ -\sin\theta & \cos\theta\sin\psi & \cos\theta\cos\psi \end{bmatrix} \tag{4-3}$$

Where ψ , θ , ϕ denote three successive rotations of the moving frame about the fixed x, y and z axes.

Combining (4-2) and (4-3), we obtain a 4 × 4 transformation matrix $\boldsymbol{T}_{\boldsymbol{B}}^{\boldsymbol{P}}$, as given below:

$$\boldsymbol{T}_{\boldsymbol{B}}^{\boldsymbol{P}} = \begin{bmatrix} \boldsymbol{R}_{\boldsymbol{B}}^{\boldsymbol{P}} & \boldsymbol{P}_{\boldsymbol{p}} \\ \boldsymbol{0} & \boldsymbol{1} \end{bmatrix} \tag{4-4}$$

Hence the six variables, denoted as $\boldsymbol{P} = \left[p_x, p_y, p_z, \psi, \phi, \theta \right]^T$, completely define the position and orientation of the moving platform.

Following the Eq. (3-5), for the actuation redundant parallel manipulator, it has 4 actuation legs. So Eq. (3-5) can be written as:

$$\left| \mathrm{O}_b\mathrm{P}_i - \mathrm{O}_b\mathrm{B}_i - \mathrm{B}_i\mathrm{D}_i \right| = \left| \mathrm{D}_i\mathrm{P}_i \right| \qquad (i = 1, 2, 3, 4) \tag{4-5}$$

Eq. (4-5) can be yielded

$$k_{i1}^2 + k_{i2}^2 + k_{i3}^2 = l_i^2, \quad (i = 1, 2, 3, 4) \tag{4-6}$$

Where

$$
\begin{aligned}
k_{i1} &= x_{p_i}^b - \left(l_b - u_i c\gamma\right) c\alpha_i \\
k_{i2} &= y_{p_i}^b - \left(l_b - u_i c\gamma\right) s\alpha_i \\
k_{i3} &= z_{p_i}^b - u_i s\gamma
\end{aligned}
\tag{4-7}
$$

Now Eq. (4-6) can be differentiated as following:

$$
\left[\boldsymbol{\delta l_i}\right] = \begin{bmatrix} \frac{k_{i1}}{l_i} & \frac{k_{i2}}{l_i} & \frac{k_{i3}}{l_i} \end{bmatrix} \cdot \begin{bmatrix} \delta x_{p_i}^b \\ \delta y_{p_i}^b \\ \delta z_{p_i}^b \end{bmatrix} \qquad (i = 1,2,3,4) \tag{4-8}
$$

The twist of the platform can be defined as

$$
\mathbf{t} = \begin{bmatrix} \boldsymbol{\omega}^T & \dot{\mathbf{p}}^T \end{bmatrix}^T = \begin{bmatrix} \delta\theta_x & \delta\theta_y & \delta\theta_z & \delta x_p & \delta y_p & \delta z_p \end{bmatrix}^T \tag{4-9}
$$

Here, we have

$$
\dot{\boldsymbol{\rho}} = \mathbf{J}\mathbf{t} = \begin{bmatrix} \delta l_1 & \delta l_2 & \delta l_3 & \delta l_4 \end{bmatrix} \theta^T \tag{4-10}
$$

And

$$
\begin{bmatrix} \boldsymbol{\delta l_1} \\ \boldsymbol{\delta l_2} \\ \boldsymbol{\delta l_3} \\ \boldsymbol{\delta l_4} \end{bmatrix} = \left(\boldsymbol{J_p}\right)_{4\times 6} \begin{bmatrix} \delta\theta_x \\ \delta\theta_y \\ \delta\theta_z \\ \delta x_p \\ \delta y_p \\ \delta z_p \end{bmatrix} \tag{4-11}
$$

Where

$$\boldsymbol{J}_{\boldsymbol{a,i}} = \begin{bmatrix} \frac{k_{i1}}{l_i} & \frac{k_{i2}}{l_i} & \frac{k_{i3}}{l_i} \end{bmatrix} \cdot \boldsymbol{J}_{\boldsymbol{i}} \qquad (\mathrm{i} = 1,2,3,4) \tag{4-12}$$

4.3 Jacobian Matrix

The actuation redundant parallel manipulator has the same constraining leg as the kinematic redundant parallel manipulator, so the passive leg Jacobian can be used directly here. Based on the Eq.(3-37), we have

$$J_4 = \begin{bmatrix} 0 & e_{42} & e_{43} \\ e_{41} & e_{42} \times r_{42} & e_{43} \times r_{43} \end{bmatrix} \tag{4-13}$$

According to the principle of virtual work, we have

$$\boldsymbol{\tau}^T \dot{\boldsymbol{\rho}} = \mathbf{w}^T \mathbf{t} \tag{4-14}$$

Since all links are also assumed to be rigid, the compliance of the mechanism will be induced solely by the compliance of the actuators. An actuator compliance matrix, **C,** is therefore defined as

$$\mathbf{C}\boldsymbol{\tau} = \Delta\boldsymbol{\rho} \tag{4-15}$$

Where $\boldsymbol{\tau}$ is the vector of the actuated joint forces and $\Delta\boldsymbol{\rho}$ is the induced joint displacement. Matrix **C** is a (4x4) diagonal matrix whose i^{th} diagonal entry represents the compliance of the i^{th} actuator.

Then the Cartesian compliance matrix becomes (Eq.(3-57))

$$\mathbf{C}_{\mathcal{C}} = \mathbf{J}_4(\mathbf{J}_p\mathbf{J}_4)^{-1}\mathbf{C}(\mathbf{J}_p\mathbf{J}_4)^{-T}\mathbf{J}^T{}_4 \tag{4-16}$$

with

$$\Delta\mathbf{c} = \mathbf{C}_{\mathcal{C}}\mathbf{w} \tag{4-17}$$

where $\mathbf{C}_c$ is a symmetrical, positive, semi-definite (6x6) matrix, as expected.

4.4 Stiffness Modeling

In order to compare between the two parallel kinematic manipulators, the same parameters have been used in this thesis to calculate their stiffness. We also fixed the moving plate in x axis certain angle and got the stiffness results in X, Y, and Z coordination directions.

α_i	$[0^\circ \quad 90^\circ \quad 180^\circ \quad 270^\circ]$	$i = 1,2,3,4$
β_i	$[0^\circ \quad 90^\circ \quad 180^\circ \quad 270^\circ]$	$i = 1,2,3,4$
r_b	50mm	
r_a	25mm	
l_i	120 mm	$i = 1,2,3,4$
γ	50°	
Spherical Joint	$\{-40^\circ \ to \ 40^\circ\}$	
Universal Joint	$\{-50^\circ \ to \ 50^\circ\}$	
Prismatic Joint (Passive Link)	50 mm	

Table 3 Redundant 3-DOF Mechanism with the Passive Leg Kinematic Parameters

In the following stiffness mesh graphs, Figure 4.3 to Figure 4.5 show the stiffness in X axis with different view angle, same as Figure 4.6 to Figure 4.8 show the stiffness in Y axis. Figure 4.9 to Figure 4.11 show the stiffness in Z axis. One can conclude that for the

stiffness in X axis, it is decreased when the magnitude of Z coordinate increases, and also the stiffness is symmetrical along Y axis. For the stiffness in Y axis, it got the maximum value at Z = 0 point, and symmetry along Y axis. For the stiffness in Z axis, the stiffness changed very little when the X and Y value change.

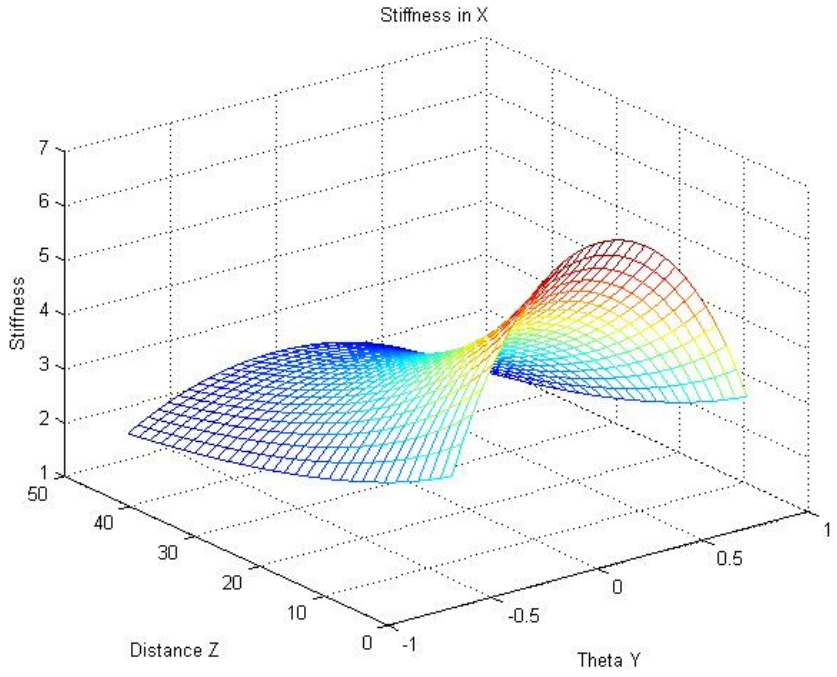

Figure 4.3 Stiffness in X axis (a)

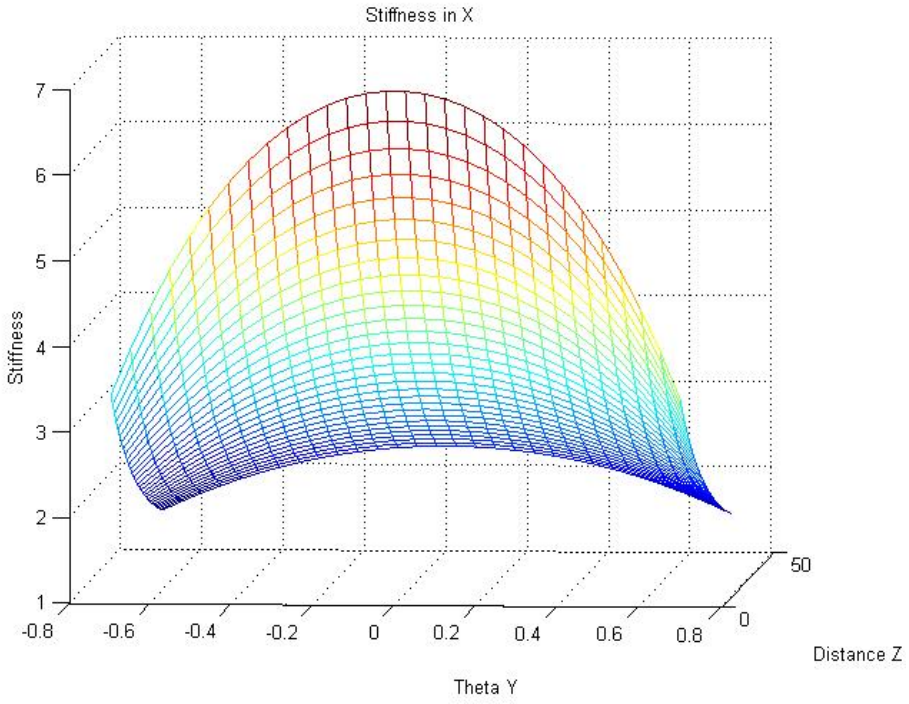

Figure 4.4 Stiffness in X axis (b)

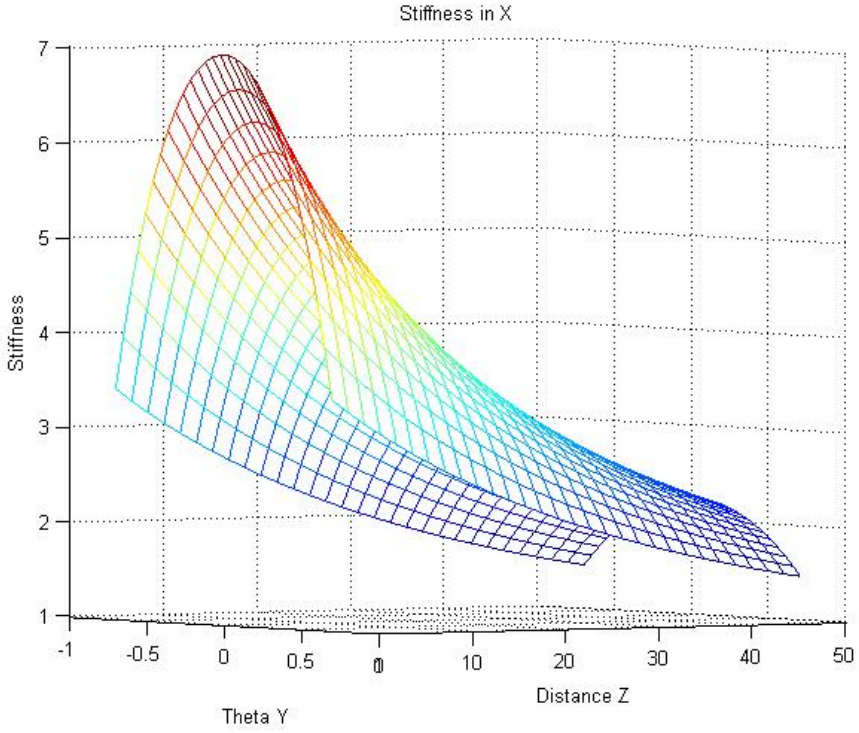

Figure 4.5 Stiffness in X axis (c)

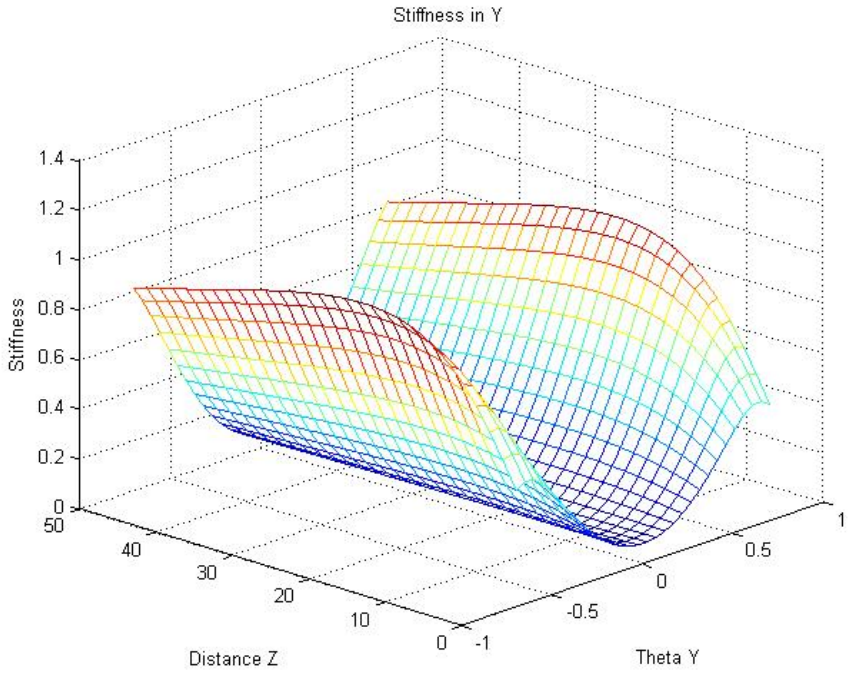

Figure 4.6 Stiffness in Y axis (a)

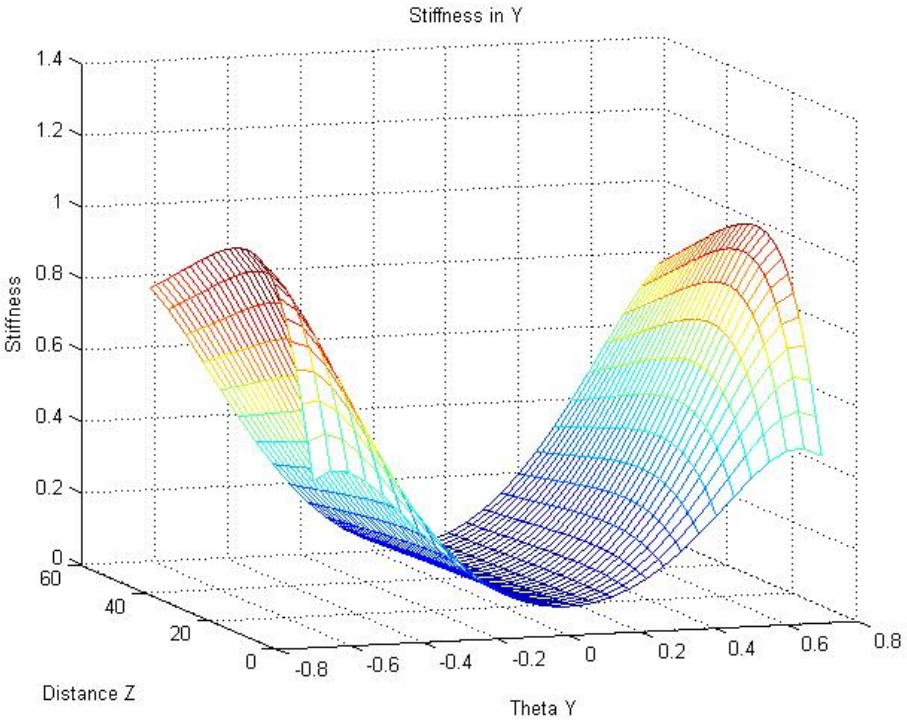

Figure 4.7 Stiffness in Y axis (b)

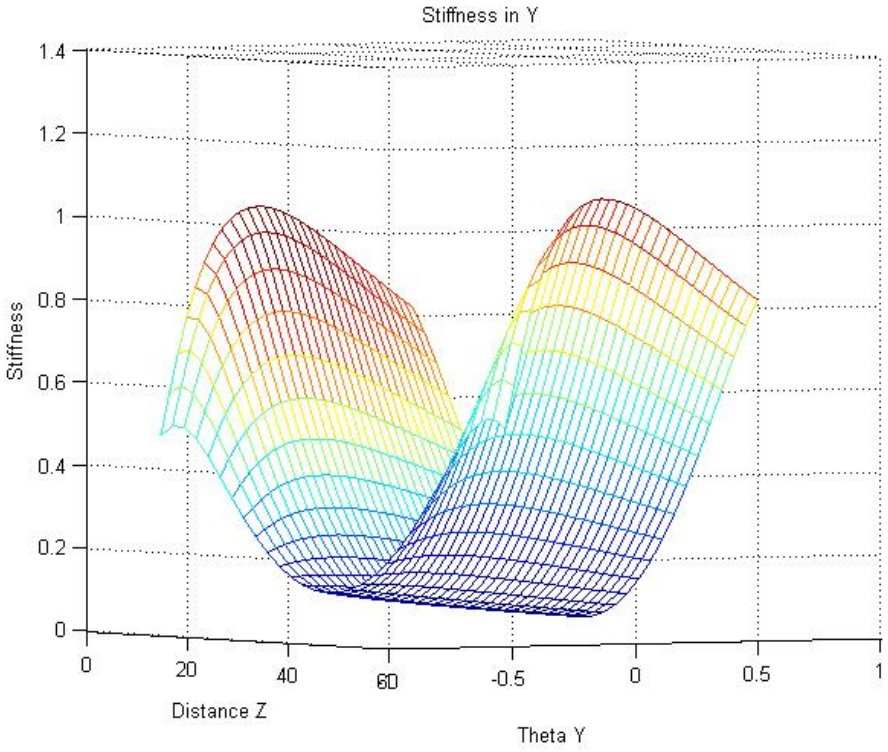

Figure 4.8 Stiffness in Y axis (c)

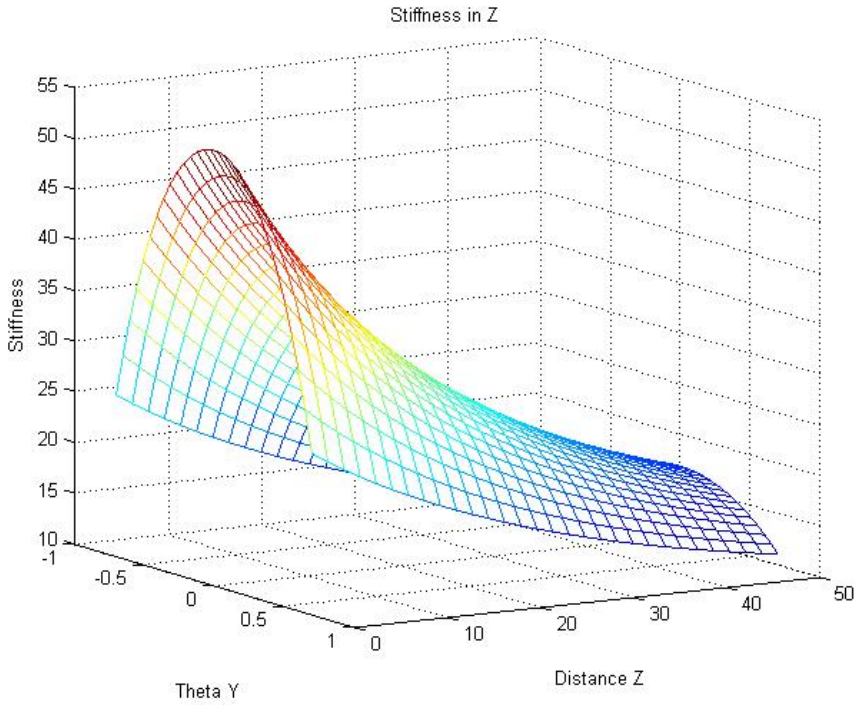

Figure 4.9 Stiffness in Z axis (a)

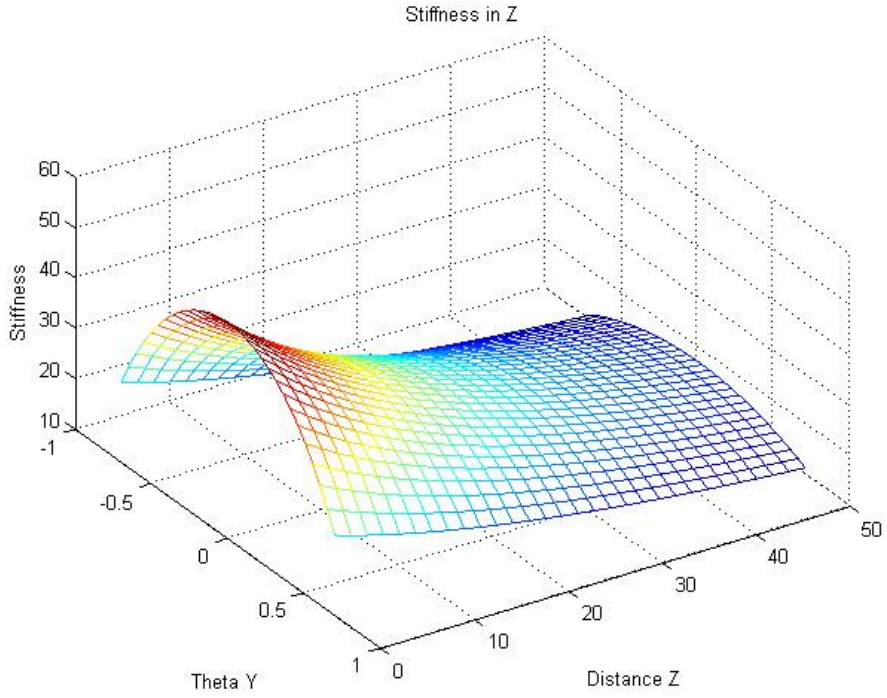

Figure 4.10 Stiffness in Z axis (b)

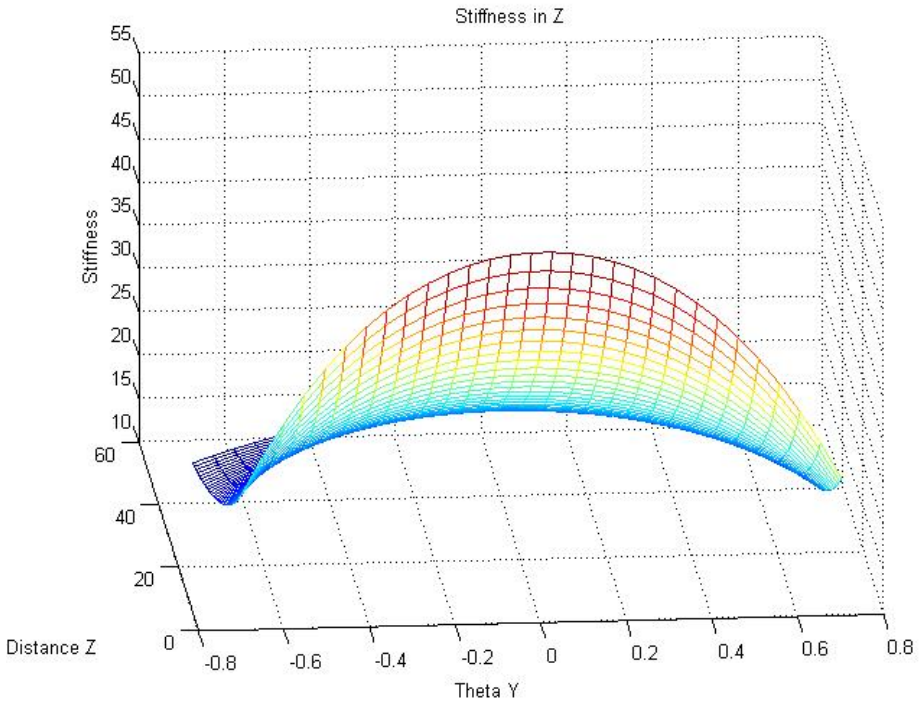

Figure 4.11 Stiffness in Z axis (c)

4.5 Conclusion

From above the stiffness mesh graphs in X (Figure 4.3 to Figure 4.5) and Y (Figure 4.6 to Figure 4.8), one can concluded that the stiffness is symmetrical in the Y axis direction, and Figure 4.9 to Figure 4.11 show that the stiffness is decreasing along z direction when the moving plate moves up. In addition, when $\theta_y = 0$, the diagrams show the maximum stiffness point, while it has a big change with varied rotation angles. That means that the position and angle of the moving platform are the main factors to determine the stiffness. The peak value of the stiffness of this redundant structure is the moving platform at Z axis lowest value point.

By comparing the stiffness mesh graphs with that of non redundant in last chapter. It is observed that the actuation redundancy has improved the stiffness of the 3-DOF micro motion parallel manipulator based on the same conditions (same overall size and actuation link size), and in the meantime it avoid the singularity problem of the micro motion parallel manipulator.

Chapter 5

Design Optimization

5.1 Introduction of Optimization Methods

The Genetic Algorithm (GA) is an excellent method for solving both constrained and unconstrained optimization problems. This algorithm repeatedly modifies a population of individual solutions based on the principle of natural selection. In each step, the Genetic Algorithm selects random individuals from the current population as parents and uses them to produce children for the next generation. Throughout each generation, the population progresses towards an optimal solution. The Genetic Algorithm can be applied to solve a variety of optimization problems, including problems where the objective function is linear, nonlinear, continuous, discontinuous, differentiable and non-differentiable.

The advantages of the Genetic Algorithm (GA) can be summarized as follows:

- Optimizes with continuous or discrete variables
- Does not require derivative information
- Simultaneously searches from a wide sampling of the cost surface

- Deals with a large number of variables
- Is appropriate for parallel computers
- Optimizes variables with extremely complex cost surfaces, especially variables that can jump out of a local minimum
- Provides a list of optimum variables rather than just a single solution

In this thesis, the GA is used for optimizing the global stiffness of the 3-DOF micro-motion parallel manipulator and the 3-DOF micro-motion parallel manipulator with actuation redundancy.

5.2 Implementation of Optimization

5.2.1 Optimization of 3-DOF Micro Motion Parallel Manipulator

n this thesis, the stiffness of a parallel manipulator is expressed by a 3 × 3 matrix. In this case, the GA is applied for optimizing the global stiffness (val) of the micro-motion parallel manipulator. The diagonal elements of the parallel manipulator stiffness matrix represent the manipulator's pure stiffness in each direction [20] (Zhang 2000). To obtain the maximum stiffness in each direction, the following objective function, which is called the fitness function for the GA, is used.

$$val = k_{11} + k_{22} + k_{33} \tag{5-1}$$

where k_{ii} $(i = 1, 2, 3)$ represents the diagonal elements of the 3-DOF parallel manipulator's stiffness matrix. Subsequently, the next objective is to maximize val in the GA.

Parameters need to be set up before the GA is utilized. First, the fitness function, which is the function of the objective being optimized, should be created. In this case, the fitness function is represented in Eq. (5-1). In order to maximize f(x), -f(x) can be minimized,

since the point at which the minimum of -f(x) occurs is the same as the point at which f(x) is maximized.

Secondly, the number of variables should be determined. In this structure, there are three design parameters, which are considered to be the optimization variables. Specifically, they include the length of the leg "*l*", the dimension of the end-effectors "r_a" and the base dimension"r_b". Furthermore, these values in Eq. (5-2) also contribute to the *val* . Therefore, the vector of optimization variables is

$$[r_a, r_b, l] \tag{5-2}$$

and their bound conditions are

$$r_a \in [18.75, 31.25] \text{ mm}, r_b \in [37.5, 62.5] \text{ mm}, \boldsymbol{l} \in [90, 150] \text{ mm},$$

The following figure displays a plot of the best and the mean values of the fitness function at each generation. The points at the bottom of the plot denote the best fitness values, while the points above them denote the mean of the fitness values in each generation. Also, at the top of the figure, the plot displays the best and the mean values for the current generation.

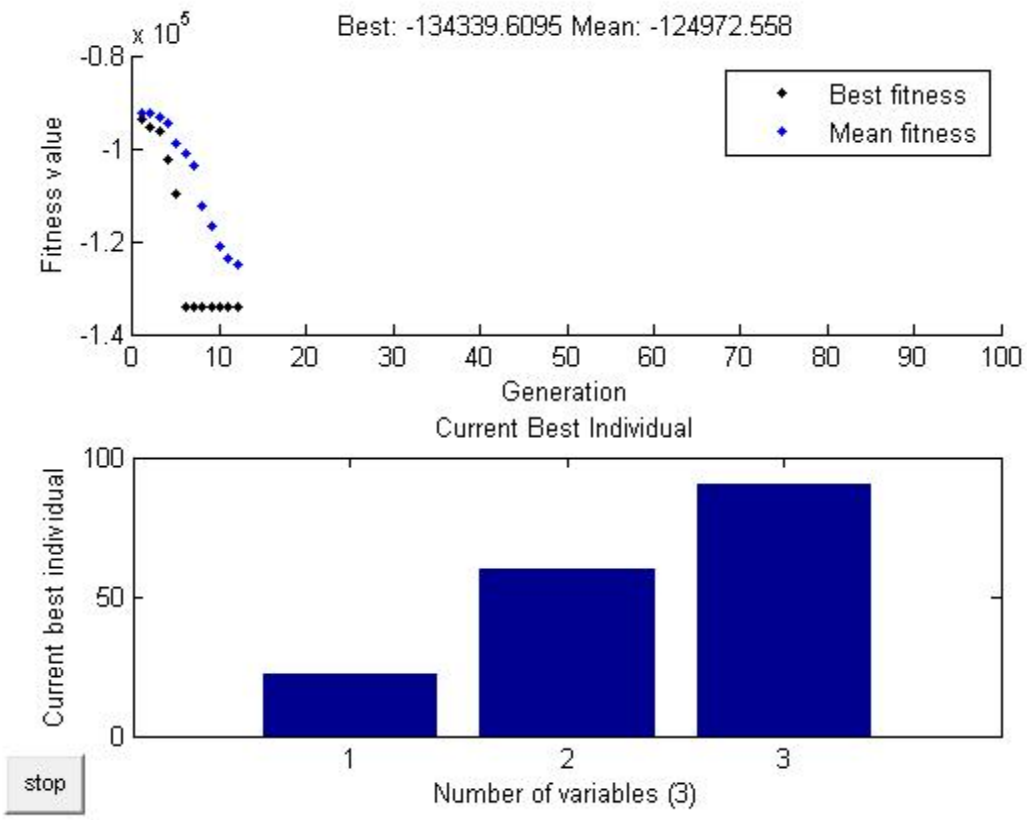

Fig 5.1: The Optimization Result for the 3-DOF Micro Motion Parallel Manipulator with the Genetic Algorithm

The optimal parameters are obtained after approximately 18 generations, and the result is expressed as:

$$[r_a, r_b, l] = [21.75mm, 59.50mm, 90.00mm]$$

With the suggested optimal design value for the length of the leg and the size of the base and moving plate, the maximum global stiffness of this structure was obtained:

$$val = k_{11} + k_{22} + k_{33} = 134339.6095(N/m)$$

	Design Parameter	Optimal Parameter	
α_i	$[-30^\circ \quad 90^\circ \quad 150^\circ]$		*i = 1,2,3*
β_i	$[-30^\circ \quad 90^\circ \quad 150^\circ]$		*i = 1,2,3*
r_a	25.00 mm	21.75mm	
r_b	50.00 mm	59.50mm	
l_i	120.00 mm	90.00 mm	*i = 1,2,3*
γ	50°		
Spherical Joint	$\{-40^\circ \quad to \quad 40^\circ\}$		
Universal Joint	$\{-50^\circ \quad to \quad 50^\circ\}$		
Prismatic Joint (Passive Link)	50 mm		

Table 4: The Optimization Results of 3-DOF Micro Motion Parallel Manipulator

In this case, the optimization parameter can be rounded as the following:

$$[r_a, r_b, l] = [22mm, 60mm, 90.00mm]$$

5.2.2 Optimization of 3-DOF Micro Motion Parallel Manipulator with Actuation Redundancy

With this structure, the same concept was used as with the 3-DOF micro-motion parallel manipulator in the previous section. The diagonal elements of the matrix represent the pure stiffness of the 3-DOF micro-motion parallel manipulator with actuation redundancy in each direction [20]. To obtain the maximum stiffness in each direction, the following objective function, which is also called the fitness function in the GA, can be written, which yields

$$val = k_{11} + k_{22} + k_{33} + k_{44} \tag{5-3}$$

where k_{ii} $(i = 1, 2, 3, 4)$ represents the diagonal elements of the PKM's stiffness matrix. The next objective is to maximize val in the GA.

There are also three design parameters considered as optimization variables, including the length of the leg "l", the dimension of the end-effectors "r_a" and the base dimension"r_b". Additionally, these values in Eq. (5-2) also contribute to the val. Therefore, the vector of optimization variables is expressed as

$$[r_a, r_b, l] \tag{5-4}$$

And their bound conditions are

$$r_a \in [18.75, 31.25] \text{ mm}, r_b \in [37.5, 62.5] \text{ mm}, \boldsymbol{l} \in [90, 150] \text{ mm},$$

The following figure displays a plot of the best and the mean values of the fitness function at 22 generations.

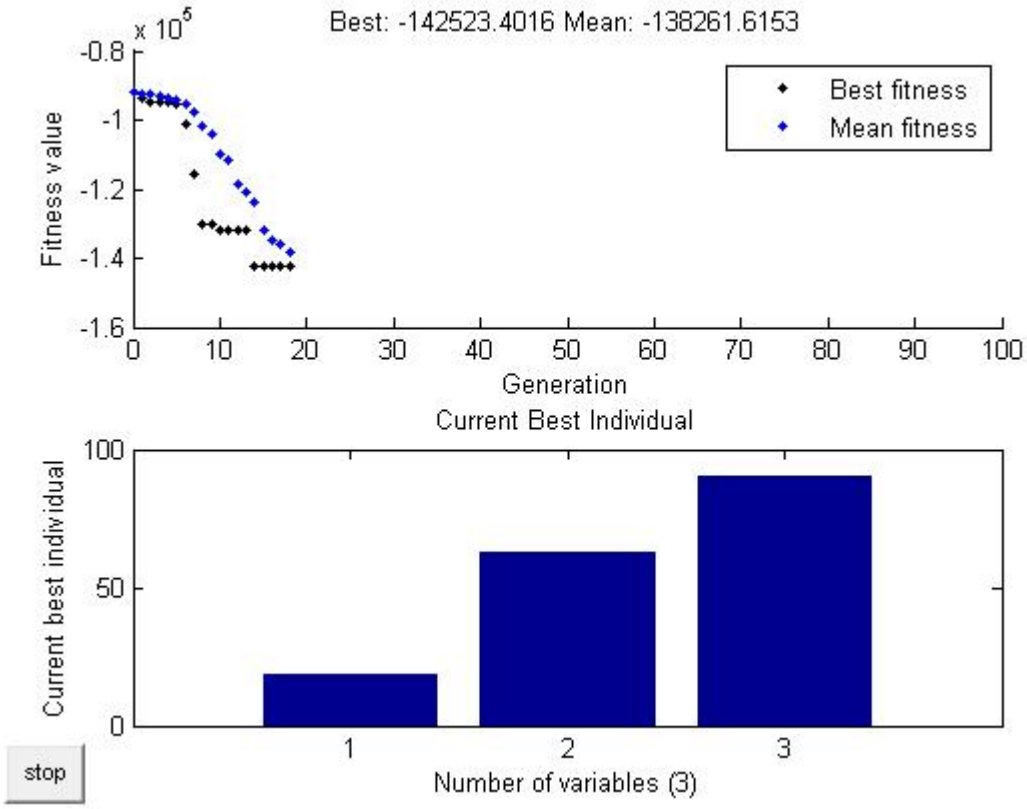

Fig 5.2: The Optimization Result for the 3-DOF Micro Motion Parallel Manipulator with Actuation Redundancy

The optimal parameters are obtained after approximately 22 generations, and the result is expressed as the following:

$$[r_a, r_b, l] = [18.75mm, 62.50mm, 90.00mm]$$

With the suggested optimal design value for the length of the leg and the size of the base and moving plate, the maximum global stiffness of this structure is

$$val = k_{11} + k_{22} + k_{33} + k_{44} = 142523.4016(N/m)$$

	Design Parameter	Optimization Parameter	
α_i	$[0^\circ \quad 90^\circ \quad 180^\circ \quad 270^\circ]$		*i = 1,2,3,4*
β_i	$[0^\circ \quad 90^\circ \quad 180^\circ \quad 270^\circ]$		*i = 1,2,3,4*
r_a	25.00mm	18.75mm	
r_b	50.00mm	62.50mm	
l_i	120.00 mm	90.00 mm	*i = 1,2,3,4*
γ	50°		
Spherical Joint	$\{-40^\circ \quad to \quad 40^\circ\}$		
Universal Joint	$\{-50^\circ \quad to \quad 50^\circ\}$		
Prismatic Joint (Passive Link)	50 mm		

Table 5: The Optimization Results for 3-DOF Micro Motion Parallel Manipulator with Actuation Redundancy

For the actual size prototyping model, the optimization parameter of the redundant structure is expressed as:

$$[r_a, r_b, l] = [18.75mm, 62.50mm, 90.00mm]$$

5.3 Conclusions

For the design optimization, the moving plate was fixed at a certain position, which meant that θ_x , θ_y, and z_b were at a certain volume, in order to determine the dimensions of $r_a . r_b$, and l_i and the maximum stiffness. Based on the positions of the moving plate, the outcomes were likely to vary. Tables 4 and 5 show the optimization results of the 3-DOF Micro-Motion Parallel Manipulator with 3 active legs and the 3-DOF Micro-Motion Parallel Manipulator with Actuation Redundancy, which has 4 active legs. These results demonstrated that with a similar design size, the stiffness of the redundant structure is 6% greater than that of the non-redundant structure.

Chapter 6

Simulation and Comparisons

In this chapter, we conducted a Finite Element Analysis and a Dynamic Study. The purpose of the FEA and the Dynamic Study is to improve the design of the structures and to optimize the model size.

6.1 Finite Element Method Analysis

Finite element method (FEM) analysis plays an increasingly important role in engineering practice, as it is relatively inexpensive and efficient in comparison with physical experiments. Currently, FEM is utilized in almost all of the engineering fields, as it is a powerful tool in predicting the ultimate loads and the complex failure modes of 3-D structural members.

In this research, the purpose of FEM is to find the maximum and minimum stress points. This section examines the three-dimensional solid models, which are developed using Unigraphics NX6.

For the FEM conditions, the reasonable press force of 25N was applied to the moving platform, and the maximum stress on the components was calculated. Subsequently, the result can be exported as the stress, strain or displacement of the specific part of the structure. In order to compare the two proposed structures, the geometric size of the manipulators was made equal. From the FEM results, the maximum and minimum deformation areas were found.

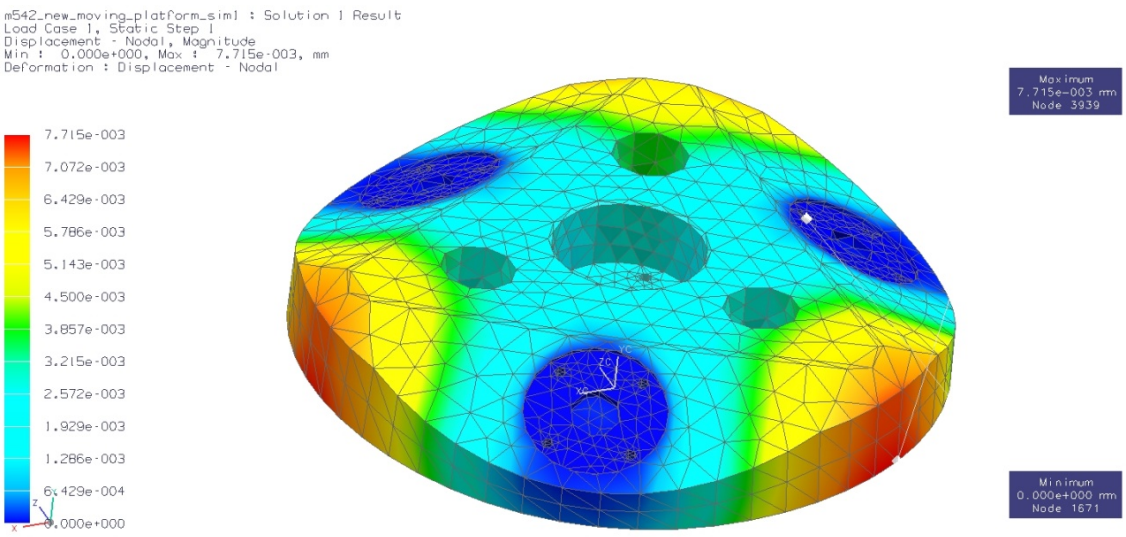

Figure 6.1: Moving Plate FEM Simulation of 3-DOF Micro Motion Parallel Manipulator with a Passive Leg

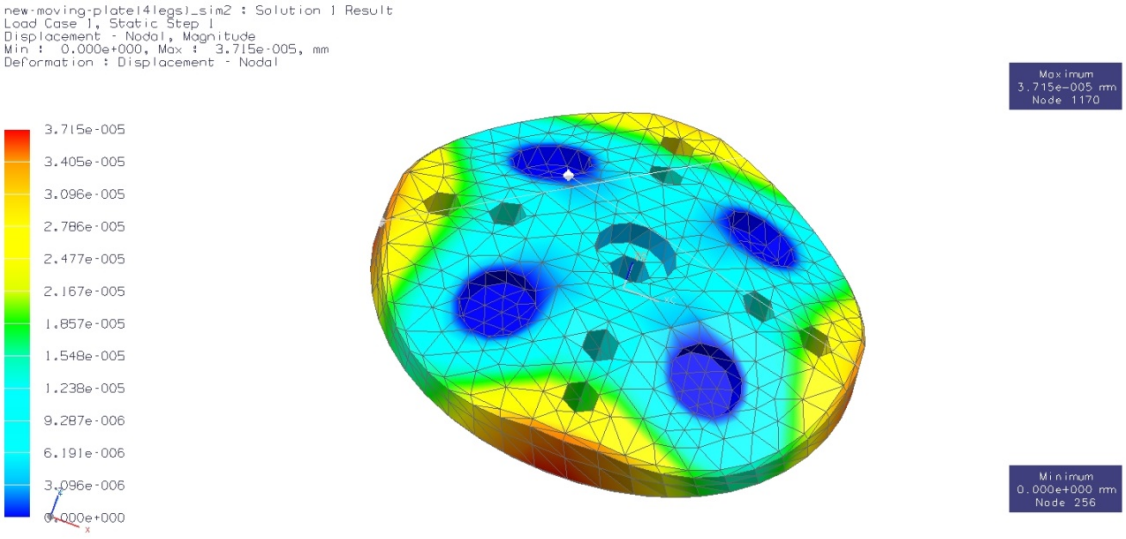

Figure 6.2: Moving Plate FEM Simulation of 3-DOF Micro Motion Parallel Manipulator with Actuation Redundancy

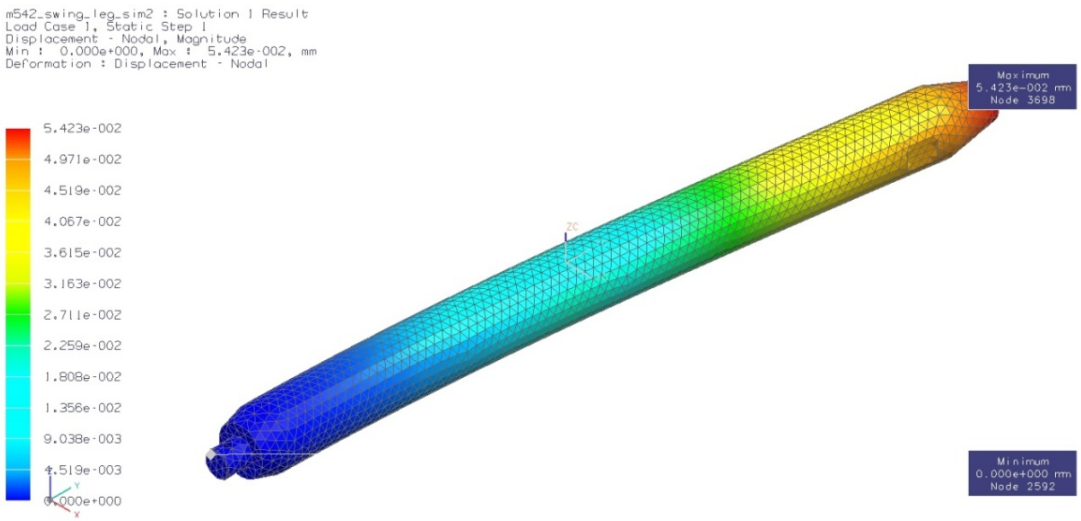

Figure 6.3: Moving Link FEM Simulation of 3-DOF Micro Motion Parallel Manipulator with Actuation Redundancy

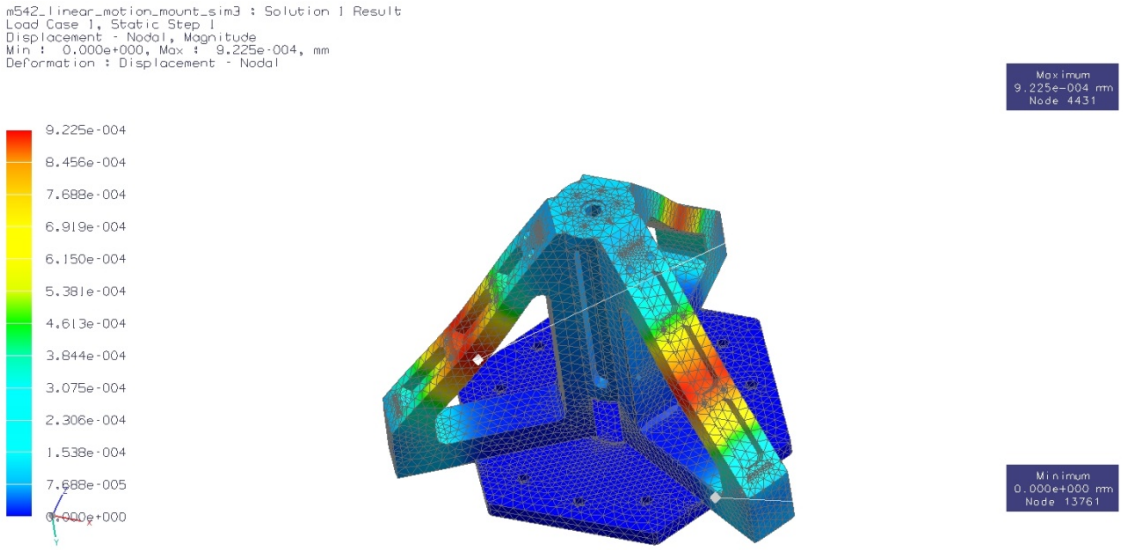

Figure 6.4: Triangle Support FEM Simulation of 3-DOF Micro Motion Parallel Manipulator

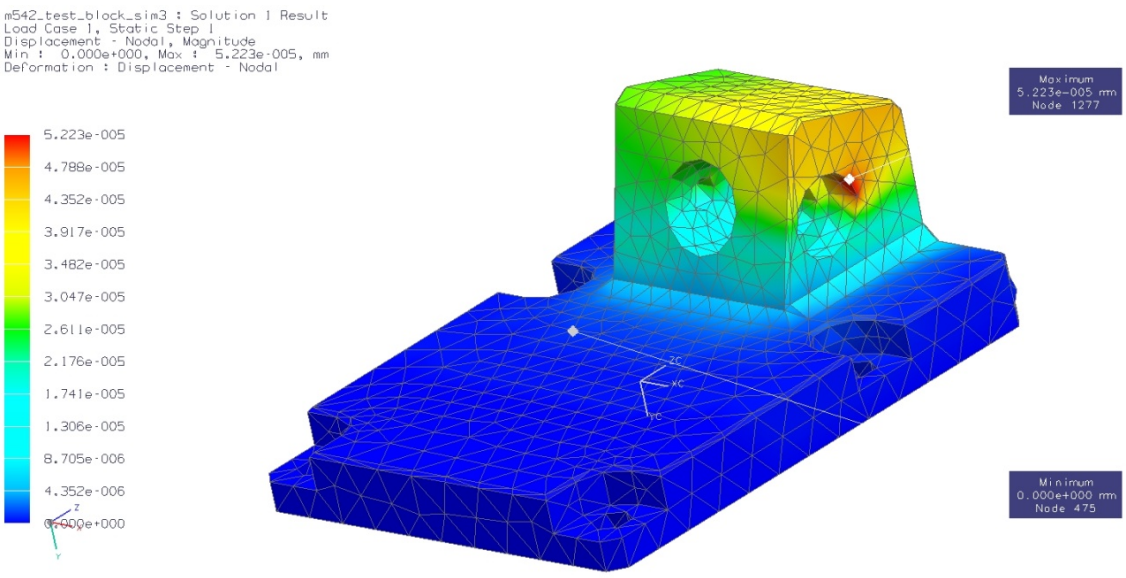

Figure 6.5: Driving Block FEM Simulation of 3-DOF Micro Motion Parallel Manipulator with Actuation Redundancy

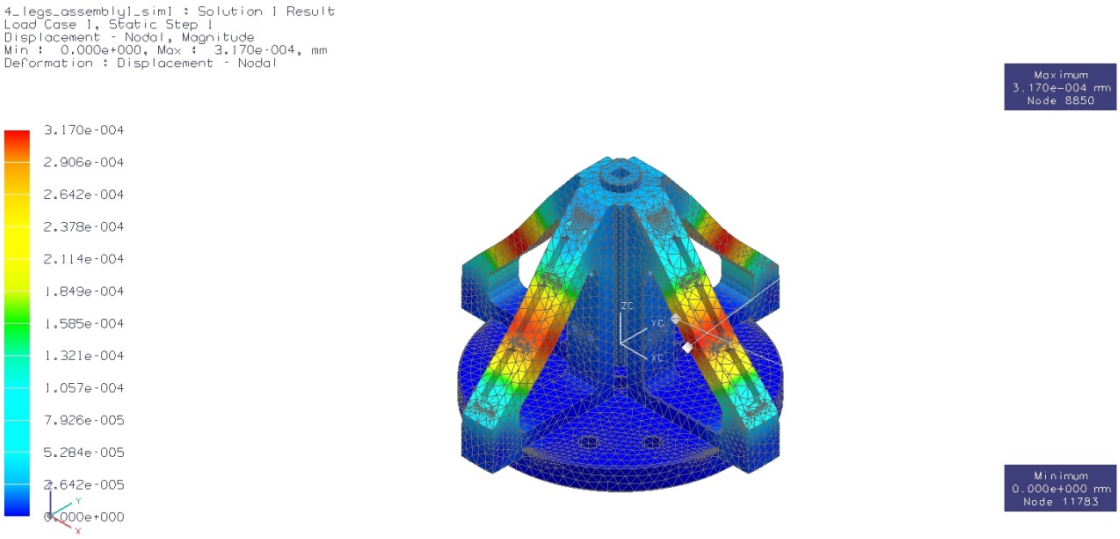

Figure 6.6: Triangle Support FEM Simulation of 3-DOF Micro Motion Parallel Manipulator with Actuation Redundancy

For each manipulator, the same amount of force was applied to the moving platform, achieving the maximum displacement, or deformation, of the triangle support. For the 3-DOF micro-motion parallel manipulator, the triangle support resulted in a peak deformation of 9.225e-004mm, whereas for the 3-DOF micro-motion parallel manipulator with actuation redundancy, the deformation was 3.170e-004mm. Furthermore, the deformation on the moving platform was obtained for each manipulator. In this case, the 3-DOF micro-motion parallel manipulator had a maximum deformation of 7.715e-0.003 mm, while the 3-DOF micro-motion parallel manipulator with actuation redundancy had a maximum deformation of 3.715e-005mm. Therefore, these results demonstrate that the 3-DOF micro-motion parallel manipulator with actuation redundancy is much more robust than the 3-DOF micro-motion parallel manipulator without redundancy.

6.2 Velocity and Acceleration Analysis

The dynamics of PKMs involve the science of studying the forces required to cause motion. To accelerate a PKM from rest to a desired speed, or to decelerate it from a certain speed to rest, a complex set of forces or torques must be applied by joint actuators. Therefore, finding the relationships between the accelerations, velocities and positions of the end-effector and the joint forces is the main task in this dynamic analysis. These relationships can

be obtained by dynamic modeling, or more specifically, by finding the dynamic equations of motion. The equations generally serve two purposes for PKMs: control and simulation. When controlling a PKM in a desired motion, the actuator torques need to be calculated using the dynamic equations of motion. On the other hand, by rearranging the dynamic equations so that the accelerations and velocities are computed as the function of the actuator forces and torques, it is possible to simulate the way in which a PKM would move under the application of actuator torques. An understanding of manipulator dynamics is important from several different perspectives. First, it is necessary to properly define the size of the actuators and the other manipulator components. Without a model of the manipulator dynamics, it is difficult to predict the actuator force requirements, and, consequently, it is challenging to properly select the actuators. Second, a dynamic model is useful for developing a control scheme. With an understanding of manipulator dynamics, it is possible to design a controller with improved performance characteristics. Moreover, some control schemes, such as the computed torque controller, rely directly on the dynamic model in order to predict the desired actuator force used in a feed-forward manner. Third, a dynamic model can be used for a computer simulation of a robotic system.

In this section, we utilize Adams/View software to run the dynamic analysis. Generally, Adams/View is used to perform the kinematic and dynamic simulations of a multi-body mechanism. In this software, the motion of a rigid body is driven by motion at a joint. Because the inverse kinematics can be presented in closed form, the motions at the three prismatic joints between the slides and the three legs are defined and input according to the position equations (3-3) and (4-3). The simulation result of the actuator force can be output, and other kinematics and dynamic analysis, such as velocity, acceleration and kinematic energy, can also be shown in Adams/View.

By applying Adams/View software to run the dynamic analysis, the displacement, velocity, acceleration and instantaneous rotation center of the platform for the parallel manipulator with three to four active links can be automatically solved and visualized, and the velocity and acceleration simulation structures of the parallel manipulators can be created similar to a 3-D sketch model. However, unlike a real 3-D solid model, when modifying the size of the active links, the configurations of the velocity and acceleration simulation results are varied accordingly, but all of the geometric and dimension constraints are always maintained; thus, all mathematical relationships of the parallel manipulators are also retained.

6.2.1 Velocity and Acceleration Analysis of 3-DOF Micro Motion Parallel Manipulator

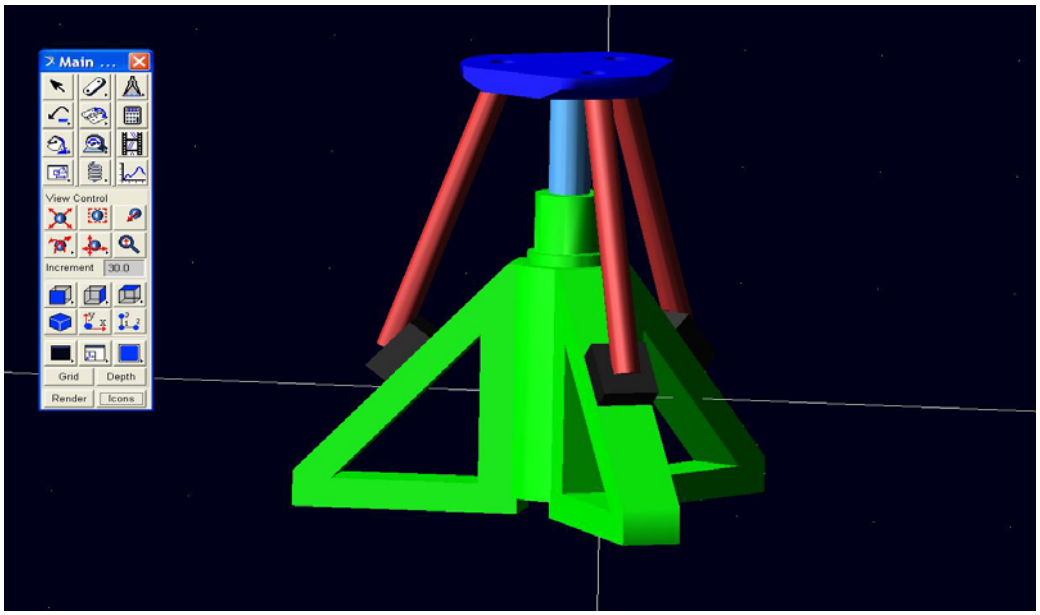

Figure 6.7: Adams/View Model of the 3-DOF Micro Motion Parallel Manipulator with Passive Leg

In the following diagrams, several abbreviations are used to represent motion terms:

Acc and Accel both represent acceleration.

P and Pos both represent displacement.

V and Vel both represent velocity.

The following graphs are generated from Adams/View. In this simulation, 7 seconds and 200-step simulations produce 4 sets of curves for the first 3-DOF micro-motion parallel manipulator. Each graph represents a particular link or platform: Figure 6.8 is the result for Link 1, Figure 6.9 shows Link 2, Figure 6.10 demonstrates the result for Link 3, and Figure 6.11 depicts the simulation result for the moving platform.

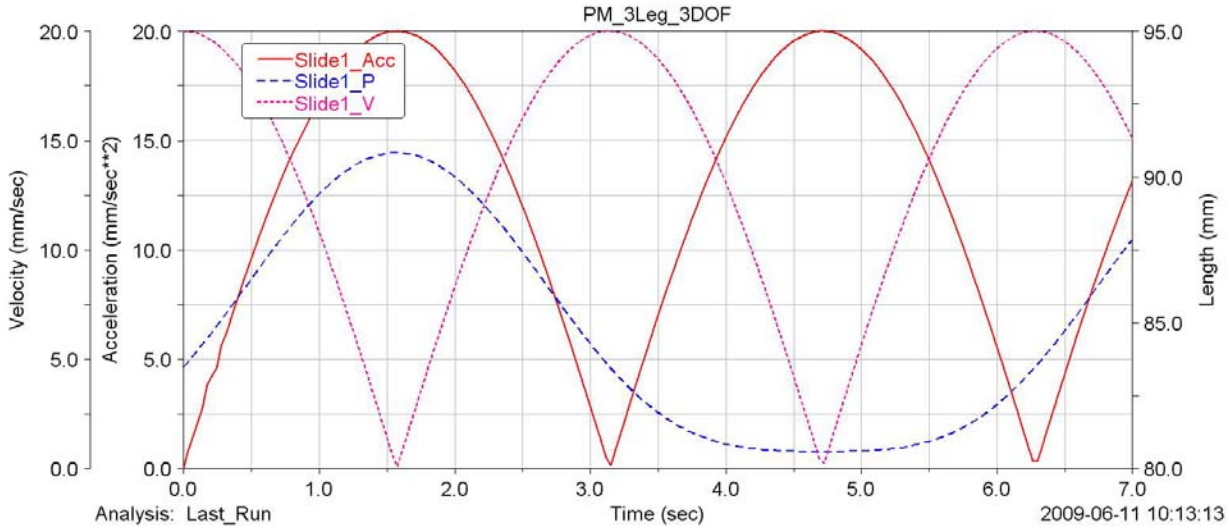

Figure 6.8: Displacements, Velocity, and Acceleration of Active Link 1

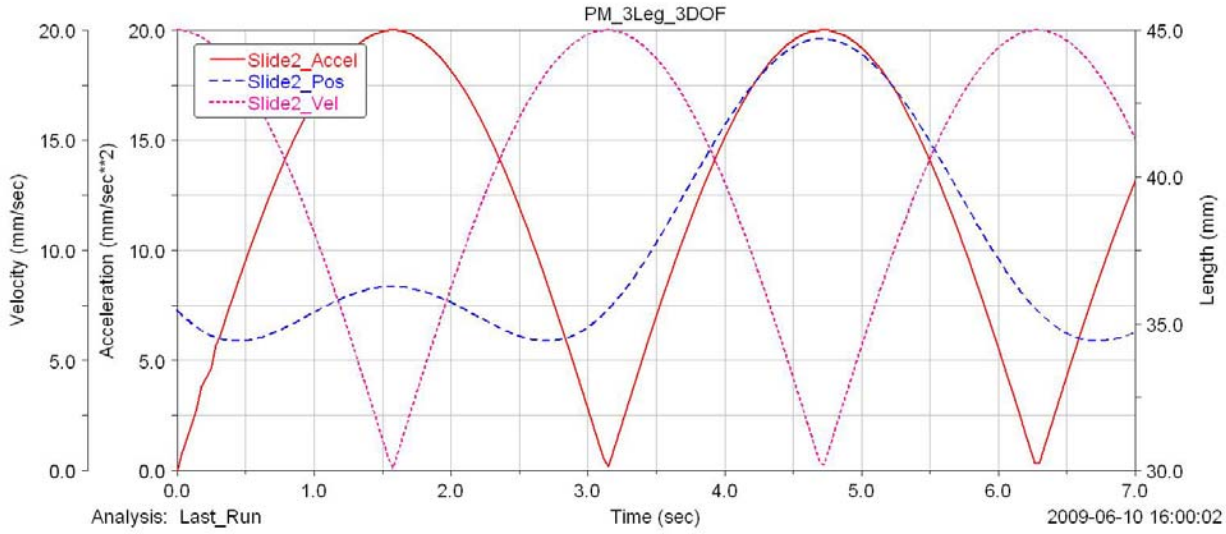

Figure 6.9: Displacements, Velocity, and Acceleration of Active Link 2

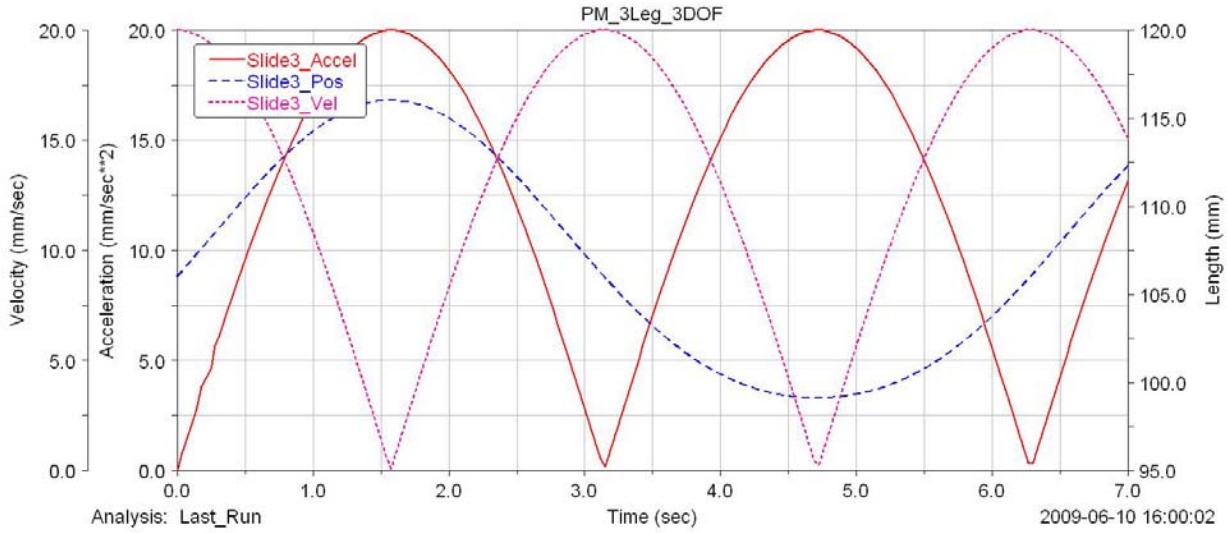

Figure 6.10: Displacements, Velocity, and Acceleration of Link 3

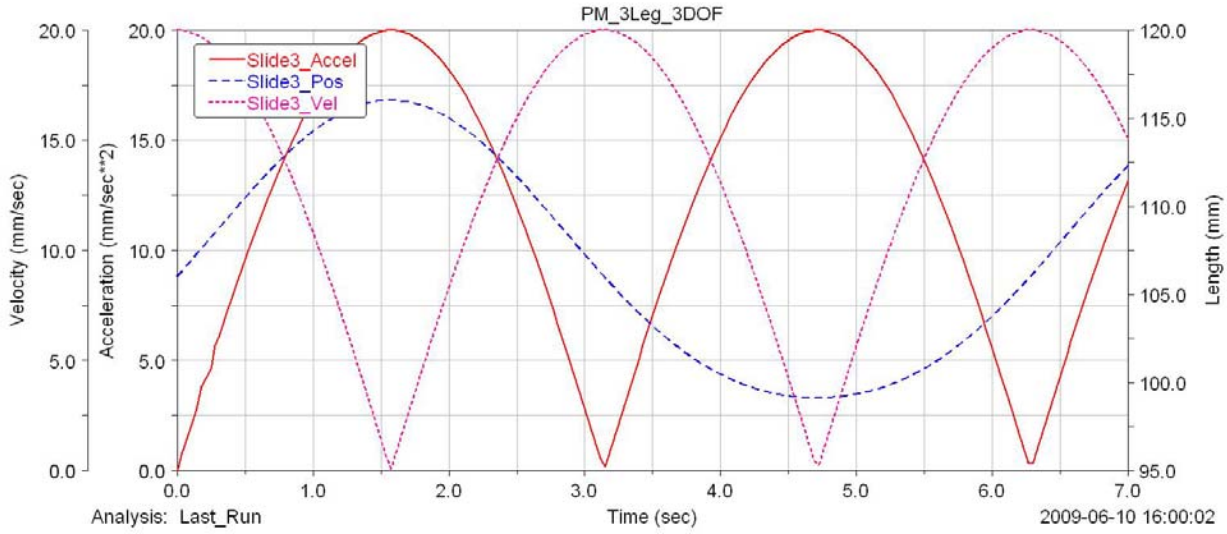

Figure 6.11: Displacements, Velocity, and Acceleration of Moving Platform

Figures 6.8 to 6.11 indicate the displacements, velocities and accelerations of the 3-DOF micro-motion parallel manipulator. The velocity and acceleration curves for Links 1, 2, 3 are similar, which is because they have an identical design and use the same actuators. Figure 6.11 shows the displacement, velocity and acceleration curves for the moving platform. Link 1 and Link 3 have the same magnitude and the same direction, whereas Link 2 has the same magnitude as the other two links, but its motion is in the opposite direction. The resulting displacement of the moving platform caused by the 3 active links is a translation about the z-axis and rotations about the x and y axes.

6.2.2 Velocity and Acceleration Analysis of 3-DOF Micro Motion Parallel Manipulator with Actuation Redundancy

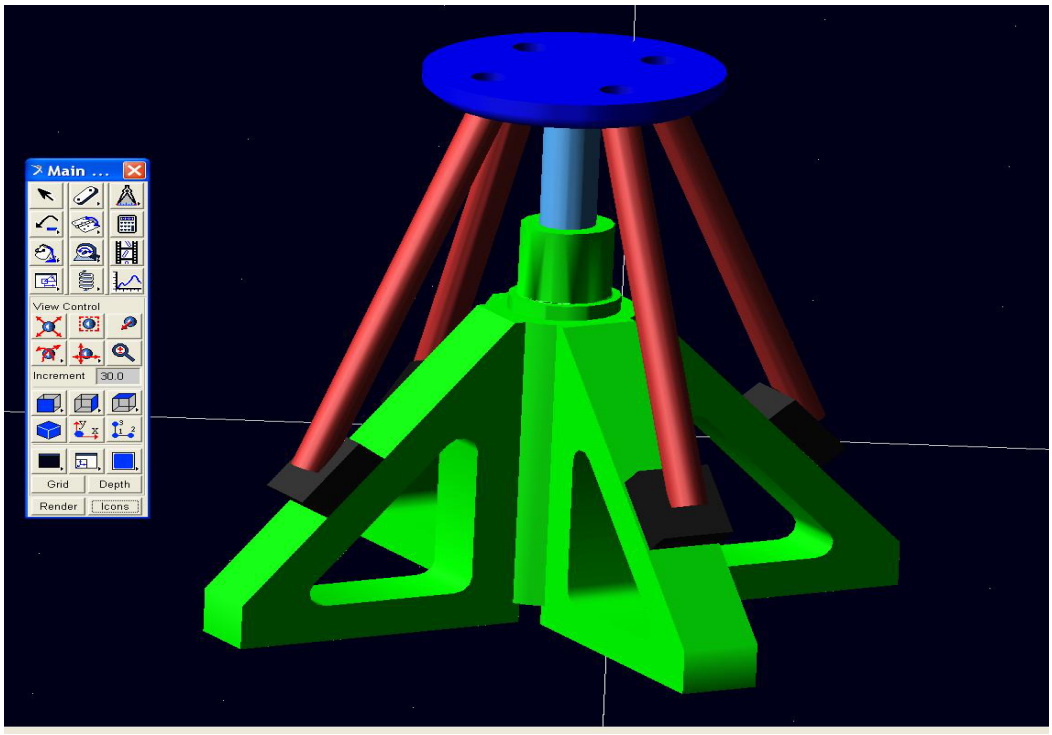

Figure 6.12: Adams/View model of the 3-DOF Micro Motion Parallel Manipulator with Actuation Redundancy

The following diagrams use the abbreviations specified below:

Acc and Accel both represent acceleration.

P and Pos both represent displacement.

V and Vel both represent velocity.

In this section, the Adams/View has been set at 7 seconds and 200 steps, and the simulations produce 5 sets of curves for the micro-motion parallel manipulator with actuation redundancy. Figures 6.13 to 6.16 show the displacement, velocity and acceleration of the four links respectively. Furthermore, the curves in Figure 6.17 provide information about the displacement, velocity and acceleration for the moving platform.

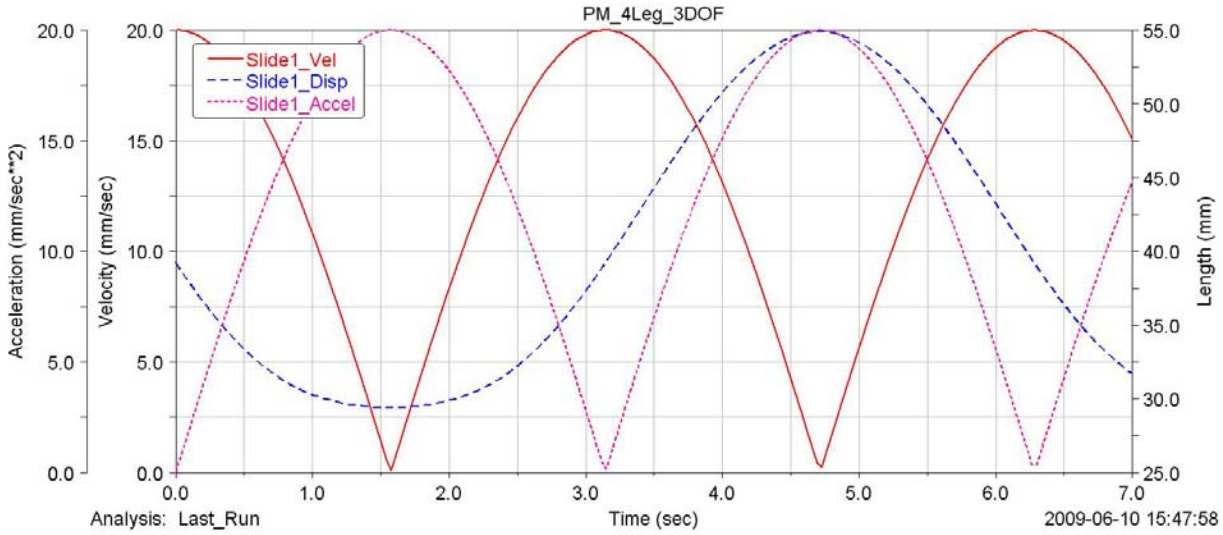

Figure 6.13: Displacements, Velocity, and Acceleration of Active Link 1

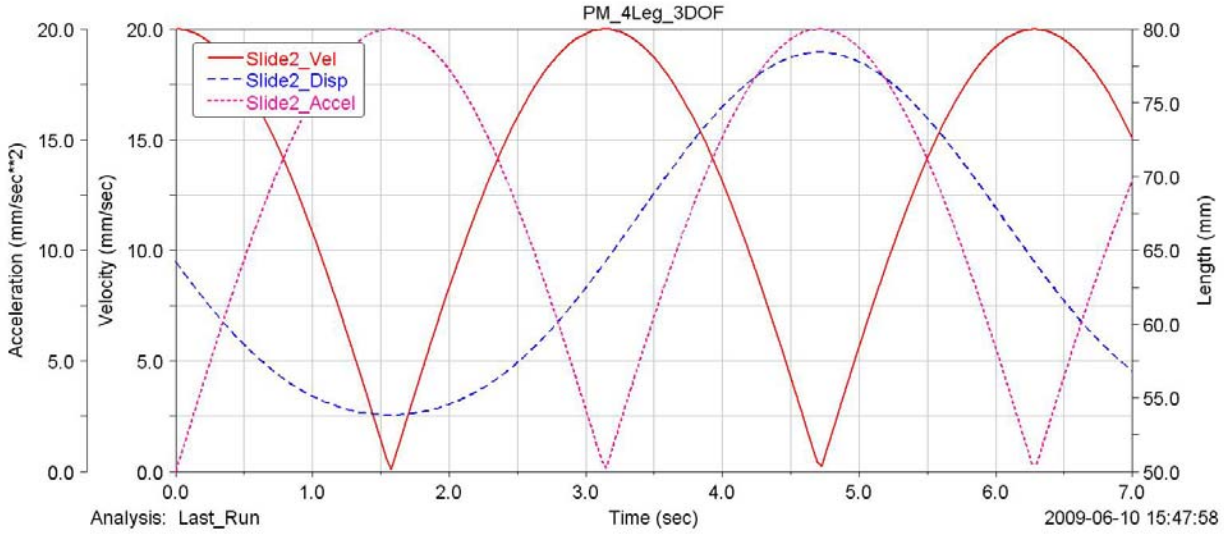

Figure 6.14: Displacements, Velocity, and Acceleration of Active Link 2

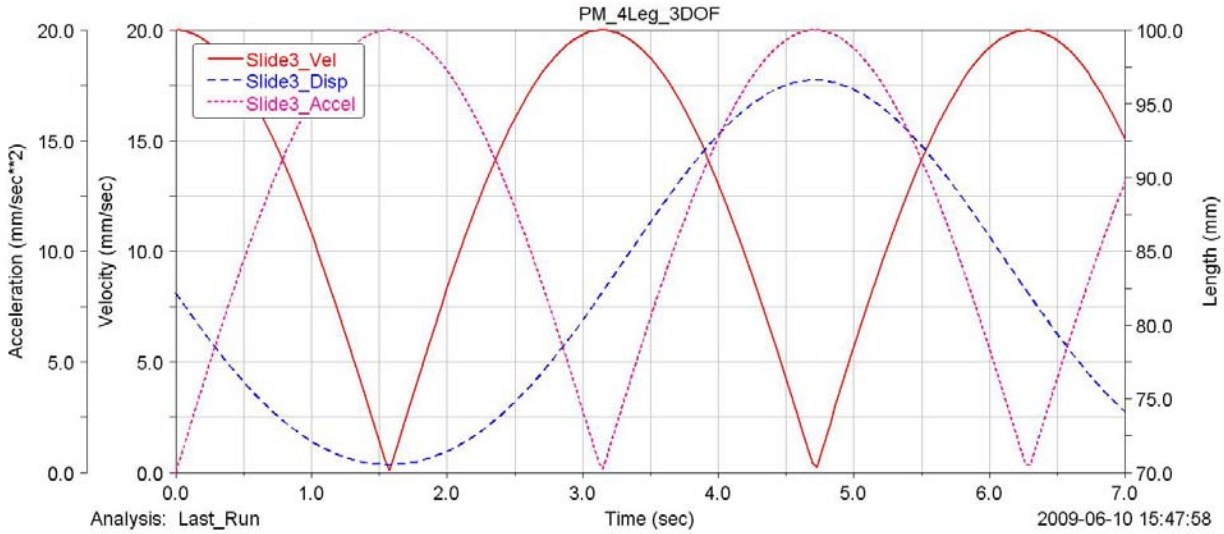

Figure 6.15: Displacements, Velocity, and Acceleration of Active Link 3

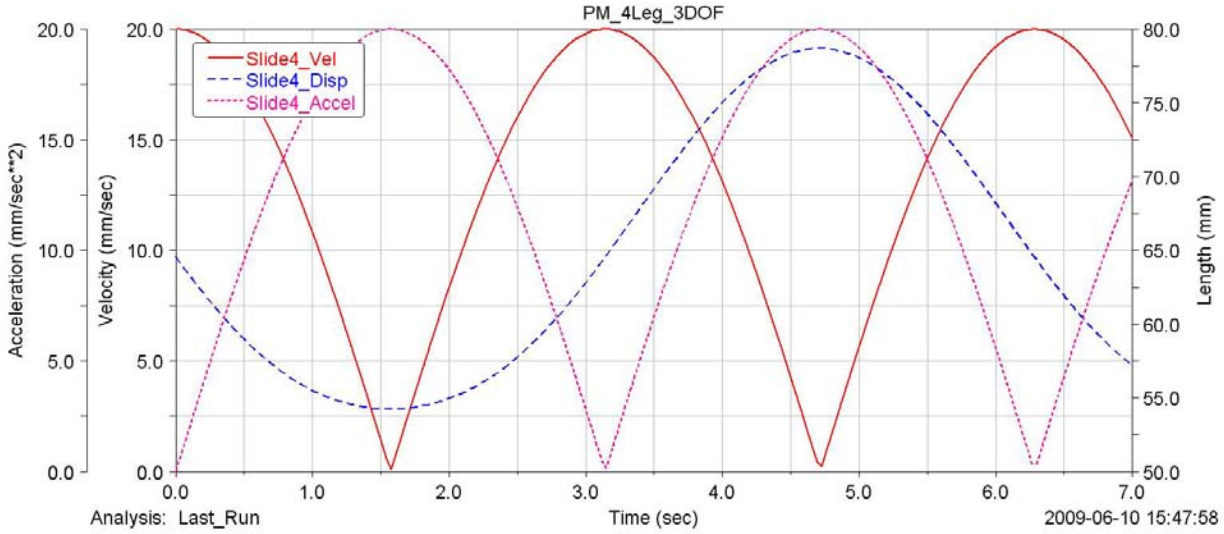

Figure 6.16: Displacements, Velocity, and Acceleration of Active Link 4

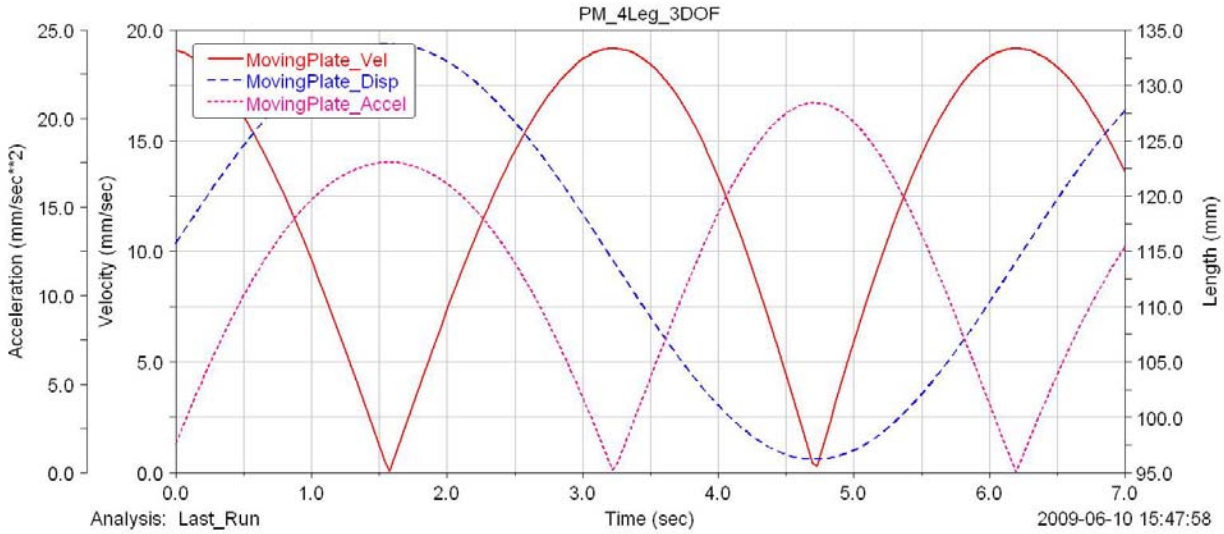

Figure 6.17: Displacements, Velocity, and Acceleration of Moving Platform

Figures 6.13 to 6.17 indicate the displacements, velocities and accelerations for the 3-DOF micro-motion parallel manipulator with actuation redundancy. The displacements,

velocities and accelerations for the four links are very similar, since the links contain an identical design and use the same actuators and these actuation links have been arranged in a symmetrical position.

The last graph shows the displacements, velocity and acceleration of the moving platform. While the velocity and acceleration of the moving platform is similar to that of the active links, the displacement is different, as it depends on the moving directions of the active links. The resulting displacement of the moving platform caused by the three active links is a translation about the z-axis and rotations about the x and y axes.

The displacement, velocity and acceleration of both structures were compared, and these two sets of graphs indicate that both results are very similar. Specifically, the curves of the redundant structure are smoother than those of the non-redundant structure, and the results of the redundant structure also show that decreasing the acceleration will reduce the force that acts on active links and joints.

Chapter 7

Conclusions and Future Work

7.1 Conclusions

This thesis proposes two newly developed micro-motion 3-DOF parallel manipulators: one of which is a 3-DOF micro-motion parallel manipulator, and another which is the 3-DOF micro-motion parallel manipulator with actuation redundancy. Throughout the thesis, the CAD models for the design have been created, the inverse kinematics for both structures have been analyzed, and the Jacobian matrix has been derived. Additionally, stiffness models and maps were presented, the optimization of global stiffness for the PKMs were performed and the optimal design parameters have been suggested. Finally, the Finite Element Method (FEM) analysis and the dynamic analysis have been performed for both structures. The conclusions can be highlighted as follows:

The CAD models for both micro-motion 3-DOF parallel manipulators have been created with Unigraphics NX6. They are designed and developed to perform the translation

along the z-axis and rotations about x and y axes. Their unique design eliminates side-effect motions, so that they only exhibit pure 3-DOF motions, and it improves the stiffness of mechanism by applying the passive link. Furthermore, the redundant structure eliminates the singularity deficiency in the system. Both inverse kinematics have been successfully examined, and the Jacobian matrix and velocity equations were fully derived. Lastly, the research is also demonstrated by the study of kinematic and dynamic models.

The stiffness analysis section presents the stiffness models and mappings of the two proposed manipulators. In comparison with the stiffness mesh graphs and contour maps, the stiffness will increase as the z-coordinate value decreases. Specifically, it will reach its maximum where the z-value obtains the smallest point. Moreover, the stiffness mappings are symmetrical along the x or y axis due to the identical actuator links designs.

For the optimization of global stiffness, the optimal parameters are obtained for the 3-DOF micro-motion parallel manipulator after 18 generations, and the optimal parameters for the manipulator with actuation redundancy are obtained after approximately 22 generations. In comparing the optimal parameters of the two manipulators, we found these values are very close, except for the stiffness function *Val*, which is much larger for the redundancy structure. Therefore, it is evident that the redundancy structure is superior to the non-redundancy structure in terms of stiffness.

FEM analysis has been used to modify the design parameters in the research. The FEM result for the main components of the two structures produced the maximum stress and strain and the displacements or deformation. Additionally, these results demonstrated that at the maximum stress and strain conditions, the displacements of the main components for the redundant structure are much smaller than those for the non-redundant structure, thus concluding that the redundant structure is more effective than the non-redundant structure. The purpose of FEM analysis is to allow a modification of the parameters and to improve structure for future applications.

Dynamics analysis is the science of studying the forces required for causing motion; it plays an important role in the trajectory generation and control of parallel robots. In the analysis of velocity and acceleration, the simulation results have been completed. The motion equations of the two 3-DOF micro-motion parallel manipulators are derived using the Lagrange Method for dynamic modeling, which can also be used for simulation and control purposes. With the simulation results, the actuator force can be output and other kinematics and dynamic analyses, such as velocity, acceleration and kinematic energy, can also be shown in Adams/View.

7.2 Future Work

A prototyping model will be fabricated according to the optimization parameters. More detailed calculations of dynamics will be performed, and the control system needs to be designed and added to the framework. In particular, Matlab and Adams/View can be used in dynamics studies to calculate the actuator force and other kinematics and dynamic parameters. The enhanced structure optimization and some of the engineering drawings will be revised and finalized for manufacturing.

Reference

[1] Cho, ChangHyun; Kang, Sungchul; Kim,Munsang; and Song ,Jae-Bok; "*Macro-Micro Manipulation with Visual Tracking and its Application to Wheel Assembly"* International Journal of Control, Automation, and Systems, vol., no.3,pp 461-468, September 2005.

[2] Golda, Dariusz; Culepepper, Martin L; "*SMALL-SCALE MICRO/ NANO-MANIPULATORS IIN PRECISION ALIGNMENT AND POSITIONING"*

[3] Liu, Dezhong; Xu, Yihua; Fei, Renyuan; "*Study of an intelligent micro-manipulator"*Journal of Material Processing Technology 139(2003)77-80.

[4] Harachima Fumio "*Integrated Micro-motion Systems: Micromachining, control, and application".*

[5] Bang, Yongbong; Lee,Kyung-min; Kook,Juho; Lee, Wonseok; and Kim, In-su; *Micro Parts Assembly system With Micro Gripper".*

[6] Zubir, Mohd Nashrul Mohd; *"Developemtn of a high precision flex-based microgripper"*Precision Enginering 33(2009) 362-270.

[7] Gilsinn, James D.; Damazo, Bradley N.; Silver, Richard; Zhou, Hui; *"a Macro-Micro System for a Scanning Tunneling Microscope".*

[8] Nomakuchi, Tamotsu "*The speech keynote in The Eleventh international Micromachine Nanotech Symposium".*

[9] Eijekl, Kees and Baba, Yoshinobu; "*The speech keynote in The Eleventh international Micromachine Nanotech Symposium".*

[10] Ouyang, P.R.; Tjiptoprodjo, R.C.; Zhang, W.J.; Yang, G.S.; *"Micro-Motion Device technology: The State of arts review"* Int .Adv.Manuf Technol. DOI 10.1007/s001

[11] Zhang, Dan; Xu, Zhengyi; Mechefske, Chris M.; and Xi, Fengfeng "*optimum design of parallel kinematic toolheads genetic algorithms" Robotiica (2004) volume 22. Pp. 77-84. ©2004* Cambridge University Press.

[12] Clavel R (1988) DELTA, "*A fast robot with parallel geometry*". In: Proceedings of the 18th International Symposium on Industrial Robots, Lausanne, Switzerland, 26–28 April 1988, pp 91–100.

[13] Sternheim F (1987) *"Computation of the direct and inverse kinematics model of the Delta 4 parallel robot".* Roboter systeme 3:199–203.

[14] Lee, K, Shah DK (1987)"*Kinematic analysis of a three degrees of freedom in-parallel actuated manipulator"*. In: Proceedings of the IEEE International Conference On Robotics and Automation, Raleigh, NC, 31 March–3 April 1987, pp 345–350.

[15] Asada H, Cro Granito JA (1985) *"Kinematic and static characterization of wrist joints and their optimal design"*. In: Proceedings of IEEE International Conference on Robotics and Automation, St. Louis, MO, 25–28 March1985, pp 91–100.

[16] Gosselin, C; Hamel J (1994) *"The agile eye: agile performance three degree of freedom camera–orienting device."* In: Proceedings of the IEEE International Conference on Robotics and Automation, San Diego, CA, 8–13 May 1994, pp 781–786.

[17] Tsai, LW; Walsh, GC, Stamper R (1996) *"Kinematics of a novel three DOF translational platform"*. In: Proceedings of the 1996 IEEE International Conference on Robotics and Automation, Minneapolis, MN, 22–28 April 1996, pp 3446–3451.

[18] Joshi, SA; Tsai, LW (2003) *"The kinematics of a class of 3-DOF, 4-legged parallel manipulators"*. Trans ASME 125:52-60.

[19] Zhang, Dan. *"On stiffness improvement of the Tricept machine tool" Robotica (2005) volume 2, pp.377-386. © 2005 Combridge University Press*

[20] Zhang, Dan. "Kinetostatic Analysis and Optimization of Parallel and Hybrid Architectures for Machine Tools." Ph.D., Laval University, 2000.

[21] Tsai, Lung-Wen "Robot Analysis: The Mechanics of serial and Parallel Manipulators" John Wiley & Sons Inc. 1999

[22] Gough, V. *"Contribution to discussion to papers on research in automobile stability and control and in tire performance"* Proceedings of the Auto. Div Instn mech. Engrs. (1965) p. 392.

[23] Kaneko, Makoto and Higashimori, Mitsuru; *"Design of 100G Capturing Robot"*

[24] Lieberman, Isador; Hardenbrook, Mitchell; Wang, Jeffery; Guyer, Richard D., Khanna, A. Jay," *SpineAssist - Miniature Robotic Guidance for Spinal Surgery – Cadaveric Efficacy Study for Time, Accuracy and Radiation Exposure".*

[25] Lobontiu, N., *Compliant Mechanisms Design of Flexure Hinges,* Florida: CRC PressLLC, 2003.

[26] Xi, F; Han, W; Verner, M; Ross, A "*Development of a sliding-leg tripod as an Add-on Device for Manufacturing", Robotica* **19**, Parts, 285-294 (2000)

[27] Wang, J.; Gosselin, C.M., 2004, "Kinematic Analysis and Design of Kinematically Redundantly Parallel Mechanisms," ASME J. Mech. Des., 126(1), pp.109-118.

[28] Mohamed, M.G; Gosselin, C.M., 2005, "Design and Analysis of Kinematically Redundant Parallel Manipulators with Configurable Platforms" IEEE Trans. Rob., 21(3), pp. 277-287.

[29] Zhang, D. and Wang, L., 2005, "Conceptual Development of an Enhanced Tripod Mechanism for Machine Tool", *Robotics and Computer-Integrated Manufacturing* 21, no. 4-5 pp. 318-27.

[30] Bi, Z. M. and S. Y. T. Lang. "Kinematic and Dynamic Models of a Tripod System with a Passive Leg." *IEEE/ASME Transactions on Mechatronics* 11, no. 1 (02, 2006): 108-111.

[31] Chablat, D. and P. Wenger. "Architecture Optimization of a 3-DOF Translational Parallel Mechanism for Machining Applications, the Orthoglide." *IEEE Transactions on Robotics and Automation* 19, no. 3 (06, 2003): 403-410.

[32] Zhang, F.; Zhang, D.; Yang, J., and Li, B., 2005, "Kinematics and Singularity Analysis of a 3-DOF Parallel Kinematic Machine.", IEEE. 29 July-1 Aug. 2005.

[33] GOGU, G. Mechanical Engineering, Research Group, France;"A Semi-Analytical Stiffness Model Of Parallel Robots From The Isoglide Family Via The Sub-Structuring Principle"*12th IFToMM World Congress, Besançon (France), June18-21, 2007*

[34] Zhang, Dan; Wang, Lihui; Lang, Sherman Y.T. "Parallel Kinematic Machines: Design, Analysis and Simulation in an Integrated Virtual Environment" *580-588/ vol.127, July 2005 ASEM*

[35] Bouzgarrou, B. C.; Fauroux, J. C.; Gogu, G., and Heerah, Y., 2004, "*Rigidity Analysis of T3R1 Parallel Robot with Uncoupled Kinematics".*

[36] Bruyninckx, H. and Hallam, J., 2005, "*The Robotics WebBook".*

[37] Callegari, M., 2006, "Dynamics Modelling and Control of the 3-RCC Translational Platform", *Mechatronics* 16, no. 10 pp. 589.

[38] Chablat, D. and Wenger, P. 2003, "Architecture Optimization of a 3-DOF Translational Parallel Mechanism for Machining Applications, the Orthoglide", *IEEE Transactions on Robotics and Automation* 19, no. 3 pp. 403-10.

[39] Chen, S. L, and You, I. T., 2000, "Kinematic and Singularity Analyses of a Six DOF 6-3-3 Parallel Link Machine Tool." *International Journal of Advanced Manufacturing Technology* 16, no. 11 pp. 835-842.

[40] Corradini, C. and Krut, S., 2003, "A Systematic Analytical Method for PKM Stiffness Matrix Calculation." Tianjin, China, August 18-21, 2003.

[41] Craig, J. 1989, Introduction *to Robotics: Mechanics and Control,* 2nd ed., Addison-Wesley Publishing Company, Inc.

[42] Deblaise, D. Hernot, X., and Maurine, P., 2006, "A Systematic Analytical Method for PKM Stiffness Matrix Calculation", Institute of Electrical and Electronics Engineers Inc., Piscataway, NJ 08855-1331, United States, May 15-19, 2006.

[43] Dunlop, G. R. and Jones, T. P., 1996, "Gravity Counter Balancing of a Parallel Robot for Antenna Aiming."ASME, 28-30 May, 1996.

[44] Ebert-Uphoff, I.; Gosselin, C. M. and Laliberte, T., 2000, "Static Balancing of Spatial Parallel Platform Mechanisms - Revisited", *Journal of Mechanical Design, Transactions of the ASME* 122, no. 1 pp. 43-51.

[45] El-Khasawneh, B. S. and Ferreira, P. M., 1999, "Computation of Stiffness and Stiffness Bounds for Parallel Link Manipulators." *International Journal of Machine Tools & Manufacture* 39, no. 2 pp. 321-342.

[46] Gao, F.; Peng, B.; Zhao, H., and Li, W., 2006, "A Novel 5-D0F Fully Parallel Kinematic Machine Tool", *International Journal of Advanced Manufacturing Technology* 31, no. 1-2 pp. 201-7.

[47] Liu, X. J. and Wang, J. 2003, "Some New Parallel Mechanisms Containing the Planar Four-Bar Parallelogram", *International Journal of Robotics Research* 22, no. 9 pp. 717-732.

[48] Liu, X. J. Wang, J. and Pritschow, G., 2005, "A New Family of Spatial 3-DoF Fully-Parallel Manipulators with High Rotational Capability", *Mechanism and Machine Theory* 40, no. 4 pp. 475-494.

[49] Masory, O. and Wang, J., 1995, "Workspace Evaluation of Stewart Platforms", *Advanced Robotics* 9, no. 4 pp. 443-61.

[50] Merlet, J. P. *Micro Parallel Robot MIPS for Medical Applications*. Vol. 22001.

[51] Mintchell, G. A. 2002, "Industrial Robots: Fast, Nimble at 30", *Control Engineering* 49, no. 11 pp. 32.

[52] Necsulescu, D. S., 1985, "*Stochastic Modelling of Robotic Manufacturing Systems*".

[53] Ouyang, P. R.C, and Zhang, W. J., 2005, "Force Balancing of Robotic Mechanisms Based on Adjustment of Kinematic Parameters", *Journal of Mechanical Design, Transactions of the ASME* 127, no. 3 pp. 433-440.

[54] Russo, A.; Sinatra, R. and Xi, F., 2005, "Static Balancing of Parallel Robots", *Mechanism and Machine Theory* 40, no. 2 pp. 191-202.

[55] Saltaren, R., 2007, "Field and Service Applications - Exploring Deep Sea by Teleoperated Robot - an Underwater Parallel Robot with High Navigation Capabilities", *IEEE Robotics Automation Magazine* 14, no. 3 pp. 65.

[56] Sanger, D. J.; Chen, J. Q.; Zhang, S. J., and Howard, D., 2000, "A General Method for the Stiffness Analysis of Manipulator Mechanisms", *Proceedings of the Institution of Mechanical Engineers, Part C (Journal of Mechanical Engineering Science)* 214, pp. 673-85.

[57] Simaan, N. and Shoham, M., 2003, "Geometric Interpretation of the Derivatives of Parallel Robots' Jacobian Matrix with Application to Stiffness Control", *Transactions of the ASME.Journal of Mechanical Design* 125, no. 1 pp. 33-42.

[58] Weck, M. and Staimer, D., 2002, "Parallel Kinematic Machine Tools - Current State and Future Potentials", *CIRP Annals - Manufacturing Technology* 51, no. 2 pp. 671-683.

[59] Wu, H, ed., 2008, *Parallel Manipulators, Towards New Applications*. Vienna, Austria: I-Tech Education and Publishing, April 2008.

[60] Yoon, W. K.; Suehiro, T.; Tsumaki, Y. and Uchiyama, M., 2004, "Stiffness Analysis and Design of a Compact Modified Delta Parallel Mechanism", *Robotica* 22, no. 4 pp. 463-475.